ADSORPTION OF METHANE AND CARBON DIOXIDE ON ACTIVATED CARBON AND METAL ORGANIC FRAMEWORKS

Chutima Sudsuansi

A Thesis Submitted in Partial Fulfilment of the Requirements

for the Degree of Master of Science

The Petroleum and Petrochemical College, Chulalongkorn University

in Academic Partnership with

The University of Michigan, The University of Oklahoma,

Case Western Reserve University, and Institut Français du Pétrole

2018

ADSORPTION OF METHANE AND CARBON DIOXIDE ON ACTIVATED CARBON AND METAL ORGANIC FRAMEWORKS

Chutima Sudsuansi

A Thesis Submitted in Partial Fulfilment of the Requirements
for the Degree of Master of Science
The Petroleum and Petrochemical College, Chulalongkorn University
in Academic Partnership with
The University of Michigan, The University of Oklahoma,
Case Western Reserve University, and Institut Français du Pétrole
2018

Thesis Title: Adsorption of Methane and Carbon Dioxide on Activated Carbon and Metal Organic Frameworks

By: Chutima Sudsuansi

Program: Petroleum Technology

Thesis Advisors: Prof. Pramoch Rangsunvigit

Dr. Santi Kulpratipunja

Assoc. Prof. Boonyarach Kitiyanan

Accepted by The Petroleum and Petrochemical College, Chulalongkorn University, in partial fulfilment of the requirements for the Degree of Master of Science.

.... College Dean

(Prof. Suwabun Chirachanchai)

Thesis Committee:

....

(Prof. Pramoch Rangsunvigit)   (Dr. Santi Kulpratipunja)

....

(Assoc. Prof. Boonyarach Kitiyanan)   (Prof. Thirasak Rirksomboon)

....

(Assoc. Prof. Vissanu Meeyoo)

ABSTRACT

5973002063:   Petroleum Technology Program

               Chutima Sudsuansi: Adsorption of Methane and Carbon Dioxide on Activated Carbon and Metal Organic Frameworks.

               Thesis Advisors: Prof. Pramoch Rangsunvigit, Dr. Santi Kulpratipunja and Assoc. Prof. Boonyarach Kitiyanan 86 pp.

Keywords: Adsorbed natural gas/ Methane adsorption/ Activated carbon/ Metal organic frameworks

       Natural gas has gain popularity for transportation among other fuels since it is the cleanest burning fossil fuel. However, the important challenge for utilizing natural gas is its comparatively low volumetric energy storage density. Consequently, a suitable natural gas storage is needed. Adsorbed natural gas (ANG) is an interesting alternative because it could be expected to reduce the cost and potential damage from compressed natural gas (CNG) and liquefied natural gas (LNG) technology. Comparative adsorption of methane and carbon dioxide on activated carbon ZIF-8, UiO-66, and MIL-53 (Al) was investigated at 35 °C and up to 100 psi. The addition of PVDF in ZIF-8 and activated carbon were also studied including 75 wt% ZIF-8, 50 wt% ZIF-8, 25 wt% ZIF-8, 50 wt% ZIF-8, and 25 wt% ZIF-8. The result shows that the methane and carbon dioxide adsorption increase with the pressure. MIL-53 shows the highest methane and carbon dioxide adsorption. The high surface area and micropore volume corresponds to the high methane and carbon dioxide adsorption. However, the high micropore volume to total pore volume ratio also contributes to higher methane adsorption in the case of ZIF-8 and UiO-66. ZIF-8 has higher methane adsorption than UiO-66 although they have about the same surface area and micropore volume. On the contrary, UiO-66 has higher carbon dioxide adsorption than ZIF-8 affecting from chemical properties such as an open metal site and an organic ligand. Moreover, ZIF-8 has the highest CH_4/CO_2 selectively because it has high surface area, high micropore volume, high micropore volume to total pore volume ratio, and proper open metal site and organic ligand.

บทคัดย่อ

ชุติมา สุดสวนสี: กระบวนการดูดซับมีเทนและคาร์บอนไดออกไซด์บนถ่านกัมมันต์และ วัสดุโครงข่ายโลหะอินทรีย์ (Adsorption of Methane and Carbon Dioxide on Activated Carbon and Metal Organic Frameworks) อ. ที่ปรึกษา: ศ. ดร. ปราโมช รังสรรค์วิจิตร ดร. สันติ กุลประทีปัญญา และ รศ. ดร. บุนยรัชต์ กิติยานันท์ 86 หน้า

ก๊าซธรรมชาติเป็นเชื้อเพลิงที่ได้รับความนิยมสำหรับใช้ในด้านการขนส่งเพราะเป็น เชื้อเพลิงที่สะอาด แต่อย่างไรก็ตาม ความท้าทายสำหรับการนำก๊าซธรรมชาติไปใช้คือก๊าซธรรมชาติ นั้นมีความหนาแน่นต่ำ ดังนั้นจึงต้องมีวิธีการสำหรับกักเก็บก๊าซธรรมชาติที่เหมาะสม ซึ่ง adsorbed natural gas (ANG) เป็นทางเลือกที่น่าสนใจเพราะสามารถลดค่าใช้จ่าย และอันตรายที่เกิดจาก เทคโนโลยี compressed natural gas (CNG) และ liquefied natural gas (LNG) ได้ งานวิจัยนี้ เป็นการศึกษาการดูดซับก๊าซมีเทนและก๊าซคาร์บอนไดออกไซด์บนถ่านกัมมันต์ ZIF-8 UiO-66 และ MIL-53 (Al) ที่อุณหภูมิ 35 องศาเซลเซียส และความดันถึง 100 ปอนด์ต่อตารางนิ้ว นอกจากนี้ยังได้ ศึกษาผลของ PVDF ที่ผสมใน ZIF-8 และถ่านกัมมันต์ ซึ่งตัวดูดซับที่ใช้ประกอบไปด้วย 75%ZIF-8 50%ZIF-8 25%ZIF-8 50%ZIF-8 และ 25%ZIF-8 โดยน้ำหนัก จากผลการทดลองพบว่าปริมาณ การดูดซับก๊าซมีเทนและก๊าซคาร์บอนไดออกไซด์เพิ่มขึ้นเมื่อความดันเพิ่มขึ้น โดย MIL-53 เป็นตัวดูด ซับที่สามารถดูดซับก๊าซมีเทนและก๊าซคาร์บอนไดออกไซด์ได้มากที่สุด กล่าวอีกนัยหนึ่งได้ว่าตัวดูดซับ ที่มีพื้นที่ผิวและปริมาตรรูพรุนขนาด micropore สูง จะสามารถดูดซับก๊าซมีเทนและก๊าซ คาร์บอนไดออกไซด์ได้มากด้วย แต่สำหรับตัวดูดซับบางชนิดที่มีพื้นที่ผิวและปริมาตรรูพรุนขนาด micropore ที่ใกล้เคียงกัน พบว่าปริมาณการดูดซับก๊าซมีเทนต่างกัน ดังตัวอย่างเช่น ZIF-8 และ UiO-88 ซึ่ง ZIF-8 สามารถดูดซับก๊าซมีเทนได้มากกว่า UiO-66 ซึ่งเป็นผลมาจากอัตราส่วนของ ปริมาณรูพรุนขนาด micropore ต่อปริมาณรูพรุนทั้งหมด แสดงว่าถ้าสารใดมีอัตราส่วนของปริมาณ รูพรุนขนาด micropore ต่อปริมาณรูพรุนทั้งหมดสูง จะส่งผลให้ดูดซับมีเทนได้มาก ในทางตรงกัน ข้าม พบว่า UiO-66 สามารถดูดซับก๊าซคาร์บอนไดออกไซด์ได้ดีกว่าก๊าซมีเทนเป็นผลมาจาก คุณสมบัติทางด้านเคมี เช่น โลหะที่ไม่อิ่มตัว และ ออร์แกนิคลิแกนด์ ยิ่งไปกว่านั้น ZIF-8 มีค่าการ เลือก CH_4/CO_2 สูงสุด ซึ่งเป็นผลมาจากพื้นที่ผิวและปริมาตรรูพรุนขนาด micropore สูง มี อัตราส่วนของปริมาตรรูพรุนขนาด micropore ต่อปริมาตรรูพรุนทั้งหมดสูง รวมทั้งมี โลหะที่ไม่ อิ่มตัว และ ออร์แกนิคลิแกนด์ ที่เหมาะสม
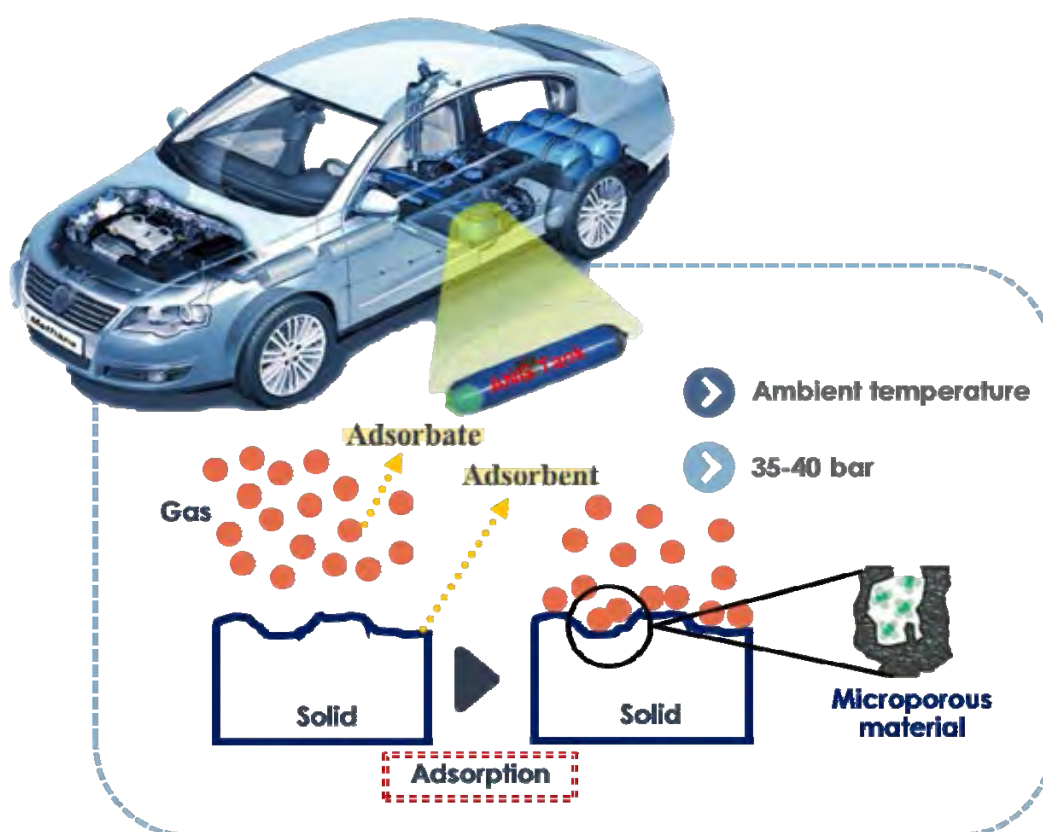
GRAPHICAL ABSTRACT

5973002063:   Petroleum Technology Program

Chutima Sudsuansi: Adsorption of Methane and Carbon Dioxide on Activated Carbon and Metal Organic Frameworks.

Thesis Advisors: Prof. Pramoch Rangsunvigit, Dr. Santi Kulpratipunja and Assoc. Prof. Boonyarach Kitiyanan 86 pp.

Keywords: Adsorbed natural gas/ Methane adsorption/ Activated carbon/ Metal organic frameworks

ACKNOWLEDGEMENTS

TABLE OF CONTENTS

LIST OF TABLES

LIST OF FIGURES

FIGURE   **PAGE**

FIGURE   **PAGE**

CHAPTER I

INTRODUCTION

According to problems from global warming by greenhouse gas emission and fluctuation of oil price, alternative energy sources are required to replace the conventional petroleum-based fuels for transportation, especially gasoline and diesel. This attraction leads to study of new clean fuels. One alternative is natural gas because of lower carbon dioxide emission, which is the major greenhouse gas and cheaper compared with gasoline (Blanco *et al.*, 2016). It is perceptible from the International Energy Outlook 2016 (IEO2016) that natural gas use as a transportation fuel was expected to increase form 2012-2040 (www.eia.gov).

Natural gas is generally composed of up to 90% of methane and various proportions of impurities such as CO_2, CO and other heavy hydrocarbons depending on the source of the gas (Rada *et al.*, 2015). Natural gas has a broad range of uses. It is used in industry, commercial, and households. It is the dominant energy used for the generation of heat and power. It can be used for cogeneration and as a motor fuel in the transport sector (CNG) (www.geoplin.si). Natural gas storage and transportation are essential in utilizing natural gas. Specifically, proper natural gas storage is needed. Potential technological options for natural gas storage include compression under high pressure (CNG), liquefaction under low temperature (LNG), and adsorbed natural gas (ANG).

Although natural gas has gained much interest as an alternative to conventional petroleum for transportation, the most important challenge for the extensive use of natural gas is its limited driving range as a result of its comparatively low volumetric energy storage density. Thus, it is necessary to use the suitable technology by increasing the energy storage density of natural gas that has ability to store an adequate amount of natural gas on vehicles. CNG is one of the current technology to solve this problem by storing natural gas as supercritical fluid at 2,900-4,350 psi and room temperature in a cylindrical tank. There are also some drawbacks from this technology. Since the storage tank of CNG has to handle high pressure, it makes them heavy and limited space form thick metal material or lighter but expensive carbon fiber and requires safety issues for use in passenger vehicles. Another

technology is LNG. It is usually stored as a boiling liquid at about -160 ºC in a cryogenic tank and 145 psi. The use of LNG is limited to the difficulties of handling a cryogenic fuel (Kayal *et al.,* 2015). For ANG, this technology is to store natural gas by adsorption in porous material at room temperature and modest pressure (507-580 psi). Among these technology, ANG technique would be better suited for use in passenger cars because it overcomes disadvantage of CNG and LNG. For instance, it is cheaper and lighter from vessel materials. Moreover, it is safe since ANG operates at room temperature and low pressure compared with CNG and LNG operating conditions (Lozano-Castello *et al.*, 2002).

Enhancement of gas storage density through adsorption depends on types of adsorbent. The requirement of highly effective ANG adsorbent is large adsorption capacity with pores size around 0.8 nm and high packing density. It has to be extremely hydrophobic and good kinetics performances, such as low heat of adsorption and high heat capacity. Additionally, contemplation of inexpensive to the end user is also importance (Lozano-Castello *et al.*, 2002). Many porous materials have been reported in literature including zeolites, activated carbon, and metal organic frameworks (MOFs). The characteristics of zeolite materials are not appropriate for using in practical vehicle applications as a result of low surface areas and extremely hydrophilic properties. Activated carbon materials have a very high surface area, narrow pore size distribution, and high energy densities contribute to high storage capacities. MOFs are a new class of microporous material, which is the most promising to storage methane with high porosity, adjustable pores and variety of factors that can improve their methane storage capacity (Li *et al.,* 2016).

Since natural gas consists of mainly methane but it is generally have some carbon dioxide, comparative study of methane and carbon dioxide is needed for the effects of carbon dioxide on methane or natural gas storage. In this work, adsorption of methane and carbon dioxide on activated carbon and MOFs consisting of ZIF-8, UiO-66, and MIL-53 (Al) were observed at room temperature and variable pressure (0-100 psi). The addition of PVDF in ZIF-8 and activated carbon for methane adsorption is also investigated. Physical properties such as surface area, micropore volume, and pore size distribution were discussed. In addition, fourier-transform infrared spectroscopy (FTIR) and scanning electron microscope (SEM) were analyzed.

CHAPTER II
THEORETICAL BACKGROUND AND LITERATURE REVIEWS

2.1 Natural Gas

Natural gas is a non-renewable resource. It can be found by itself or in association with oil. It is both colorless and odorless. It is one of the cleanest, safest, and most useful forms of energy in our daily lives (www.energy.alberta.ca). Natural gas is a naturally occurring gas mixture, consisting mainly of methane ranging from 55 to 98 percent in volume. Also, it contains ethane (C_2H_6), propane (C_3H_8), and heavier hydrocarbons. Moreover, some impurities may occur in natural gas like hydrogen sulfide, nitrogen, and carbon dioxide as showed in Figure 2.1 (Solar *et al.*, 2010). These impurities are removed before the natural gas is delivered to our home and businesses.

Natural gas occurs deep beneath the earth's surface. It is a fossil fuel. This means it originates from the remains of plants and animals that lived many millions of years ago. Heat and pressure make chemical changes over time and transform the organic matters into hydrocarbons (www.imperialoil.ca). In some places, natural gas immigrated into large cracks and spaces between layers of overlying rock. In other places, natural gas occurs in the tiny pores (spaces) within some formations of shale, sandstone, and other types of sedimentary rock, where it is referred to as shale gas or tight gas. Natural gas also occurs in coal deposits and is called coal bed methane (www.eia.gov). Natural gas that is economical to extract and easily accessible is considered "conventional". Mostly, natural gas is transported to terminals via pipelines.

Natural gas can be used in many ways. It is used to generate electricity for households and industries. It is a raw material to produce chemicals, fertilizer, hydrogen and used as a fuel for heating in industries. It is used to heat our water, cook our food, and warm our home. It is also an alternative fuel for transportation because natural gas is more environmentally friendly than conventional fuel like gasoline and diesel (www.eia.gov). From the International Energy Outlook 2016 (IEO2016), it

shows the trend of natural gas consumption of the world from 2012 to 2040 that increases from 120 trillion cubic feet (T_{cf}) to 203 T_{cf} as you can see in Figure 2.2. By energy source, natural gas accounts for the largest increase in world primary energy consumption. Abundant natural gas resources and robust production contribute to the strong competitive position of natural gas among other resources.
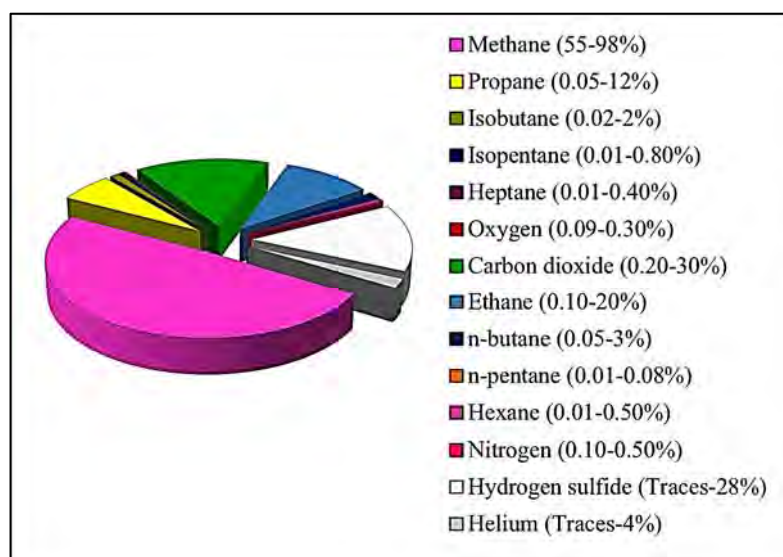
Figure 2.1 Principal constitutes of natural gas (in percentage) (Solar *et al*., 2010).
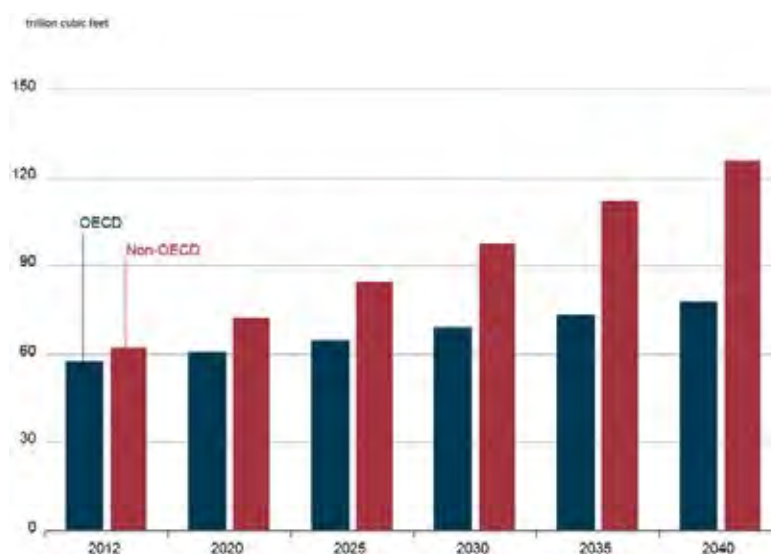
Figure 2.2 World natural gas consumption, 2012-2040 (www.eia.com).

Table 2.1 Properties of natural gas, gasoline and diesel (auto.howstuffworks.com)

Property	Natural Gas	Gasoline	Diesel
Flammability Limits (volume % in air)	5-15	1.4-7.6	0.6-5.5
Auto-Ignition Temperature (^{o}C)	450	300	230
Peak Flame Temperature (^{o}C)	1,884	1,977	2,054

2.2 Natural Gas Vehicles (NGVs)

The natural gas used in natural gas vehicles is the same natural gas that is used in domestic sector for cooking and heats. Natural-gas vehicles use the same basic principles as gasoline-powered vehicles. In other words, the fuel (natural gas in this case) is mixed with air in the cylinder of a four-stroke engine and then ignited by a spark plug to move a piston up and down. Although there are some differences between natural gas and gasoline in terms of flammability and auto ignition temperatures (Table 2.1), NGVs themselves operate on the same fundamental concepts as gasoline-powered vehicles (auto.howstuffworks.com).

Natural gas is more advantageous than other hydrocarbon fuels in several reasons. Firstly, increasing of strict environmental regulations in each country leads to find alternative fuels that can reduce greenhouse gas emissions. Natural gas is more beneficial than other hydrocarbon fuels because it burns cleaner and offers a greater reduction in carbon monoxide, nitrogen oxides, and non-methane hydrocarbon emissions while having a higher thermal efficiency and practically no particulates compared to gasoline (Zakaria and George, 2011). Secondly, it is relatively cheaper price compared to conventional and other alternative fuels. Natural gas is expected to be priced at a large discount to oil in the long term since natural gas adds to energy security at a very affordable price in countries like the United States, due to the prospect of exploring shale gas reserves in their continental shelf (Bimbo *et al.*, 2015).

Moreover, it is available in large quantities in many countries and diversification of energy resources for the automotive transportation sector. The natural gas reserves are higher than oil reserves (www.edis.sk). It is expected to be an increasing demand as a result of clean energy and cheaper than other fuel. 80%-90% of the natural gas used in US is domestically produced as it can be drawn from wells or extracted in conjunction with crude oil production. An extensive network of natural gas pipelines is already in place to deliver fuel directly to many sites including individual homes (Shen *et al.*, 2015). In addition, technology for natural gas engines has continued to develop, closing the performance gap to diesel and new generation of vehicles are becoming more attractive for operators. Finally, Gasoline and diesel must be passed through the complex refining process, while natural gas needs very less processing from field to the vehicle engine.

Even though natural gas has many advantages for using for vehicle engines, there are also some challenges, for example, substantial up-front vehicle costs, limited places to refuel, limited vehicle selection and longer refueling times but the most important challenge of using natural gas in vehicles is the comparatively low volumetric energy storage density at ambient condition. The ensuring problem is how to store enough fuel aboard the vehicle, in order to secure an acceptable driving range. On volumetric basis, 1 cubic meter of natural gas roughly corresponds to 1.0 liter of gasoline or 1.1 liter of diesel. Considering the limited space availability on-board the vehicles, a storage technology options include compression under high pressure (CNG), liquefaction under low temperature (LNG) or combination between both of them. Therefore, the potential technological methods are become the interesting and attractive way to storage and transport natural gas (www.edis.sk).

2.3 Natural Gas Storage Method

To achieve an acceptable vehicle range between refueling, it is necessary to densify natural gas because methane in its gaseous form has a density of 15.4 g/m^3 at standard temperature and pressure compared to gasoline, which has a density of 744,000 g/m^3 (Curran *et al.,* 2014). There are three different ways for on-board natural

gas storage by increasing volumetric energy density namely compressed natural gas (CNG), liquefied natural gas (LNG), and adsorbed natural gas (ANG).

2.3.1 Compressed Natural Gas (CNG)

Natural gas has been used as a transportation fuel in the form of CNG for many years in the United States and around the world, though in the United States only approximately 0.1% of the total natural gas consumption is in the form of a transportation fuel. CNG is odorless, colorless, and tasteless. An odorant is normally added to CNG for safety reasons. Natural gas compression is often done at a refueling station using industrial compressors and storage tanks. The CNG flows through a fuel line from the compression tanks into a regulator and from there, it gets injected into the engine just like gasoline (Curran *et al.*, 2014). CNG is produced by compressing the conventional natural gas (which is mainly composed of methane) to less than 1% of the volume it occupies at standard atmospheric pressure that brings its energy density to about 26% of that of gasoline. It is stored and distributed in a rigid container at a pressure of 2,900-3,600 psi, usually in cylindrical shapes metallic cylinder. The octane number of natural gas is ranging from 120 to 130. Due to this high value of octane number, CNG has a higher knock resistance than gasoline which enables the use of higher compression ratio and thus higher engine efficiency (Khan *et al.,* 2015).

CNG has been commercialized worldwide, but there are some drawbacks from its high operating pressure

1. The storage tanks are limited space and heavy weight due to bulky high-pressure cylinders (about 1 kg per liter for steel tank).

2. The high pressure system requires complex compressors, which consume high energy that is high capital cost for fuel supply compressors.

3. It is perception of danger associated with the high-pressure systems like cylinder corrosion and possibility of explosive release of compressed gas.

2.3.2 Liquefied Natural Gas (LNG)

LNG is a way of transporting natural gas long distances when pipelines are not an option-across oceans. LNG is an odorless, colorless, non-toxic, non-corrosive natural gas. Producing LNG involves compressing and cooling natural gas

to around -162 °C. That process converts the gas to a liquid and cuts its volume to 1/600th of the original, making it possible to ship the LNG in special tankers. Once it gets to its destination, the LNG can be unloaded at a receiving terminal and regasified-turned back into a gas. It can then be delivered through local pipelines to customers (www.ucsusa.org).

For heavy-duty vehicle applications, cryogenically cooling natural gas to LNG (liquefied natural gas) at -162 °C and atmospheric pressure (145 psi) increases the density but adds substantially to the cost (Khan *et al.*, 2015). The volumetric energy density of LNG is about 66 percent of total gasoline. The advantage of LNG is that it offers an energy density comparable to petrol and diesel fuels, extending range, and reducing refueling frequency (Khamechi *et al.*, 2012).

There are some drawbacks for LNG storage from large tanks. LNG transportation (usually a 70 m diameter tank, 45 m high, which can hold 100,000 m^3) requires large and expensive infrastructure. Long term storage is also difficult for LNG, as significant losses occur due to warming up and boiling off too fast (Bimbo *et al.*, 2015) because the LNG increases inevitably the temperature within the tank, the pressure rises and could result in a dangerous situation. Moreover, the filling of the tank must be performed by an expert on cryogenic liquids handling (Solar *et al.*, 2010).

2.3.3 Adsorbed Natural Gas (ANG)

Because the use of natural gas for transportation requires compressing, liquefying, or conversion, it is important to determine the best use of natural gas as a transportation fuel. ANG could be expected to answer these problems of CNG. With ANG, natural gas can be reversibly stored in porous material (adsorbent) without any chemical bonding as an adsorbed phase. Natural gas adsorption on the adsorbent has the advantage of operating at modest pressure (507-580 psi) and room temperature which is above vapour-liquid critical temperature of -83.15 °C of methane. This pressure system is obtainable by single-stage compression and room temperature, allowing natural gas stored in the tank at the same amount of high pressure storage container (Lozano-Castello *et al.*, 2002). As shown in Figure 2.3, this graph illustrates that the volumetric density of all adsorbent is higher than compress natural gas at the

same condition (Beckner and Dailly, 2016). The relatively lower pressure would make tanks lighter, cheaper, and smaller and thus reduce the cost and space requirements. Therefore, ANG technology would be better acceptable for use in passenger cars.

The performance of ANG technology not only relates to the amount of methane adsorbed but also depends on the amount of methane can be delivered to an engine. Delivery capacity is indicated as the volume of gas discharge per volume of storage tank. In practical, delivery capacity is more important than the amount of methane storage due to it indicates the driving range of natural gas vehicles (NGVs). Thus, maximization of methane adsorption and low limiting delivery capacity are two key functions that define the delivery capacity. The delivery capacity or working capacities of adsorbents also associate with thermal effects from adsorption and desorption. Adsorption is favourable at low temperature adsorbent bed due to exothermic process (Shen et al., 2015). In contrast, desorption is favourable at high temperature adsorbent bed due to endothermic process. For example, when the releasing of heat during adsorption is not efficiently dispersed or offset, there are over heat in adsorbent bed which results in less methane adsorbed at that pressure. Similarly, when the heat from adsorption cannot recycle during discharge, the temperature of adsorbent bed is not high enough resulting in more methane maintained in adsorbents at low pressure. These factors significantly decrease the working of adsorbent. Thus, it is necessary to improve strategy for reducing losses in working capacity as less as possible (Li et al., 2016). In addition, the total storage capacity is always greater than the delivery capacity by around 15-30% (Shen et al., 2015).

Figure 2.4 presents charge and discharge profiles that the temperature significantly increases during adsorption with storage pressure around. Heat generated during adsorption is dissipated for limiting maximum temperature before gas storage finishes at 35 bar. After finishing the filling process, the pressure and temperature drop. Actually, the pressure drops to 5-10 bar according to inlet pressure of NGVs. In this state, a large amount of methane is still left in the vessel. Then, the temperature turns to thermal equilibrium by exchanging with surroundings and a lot of gases are slowly desorbed for a long time (Zakaria and George, 2011).
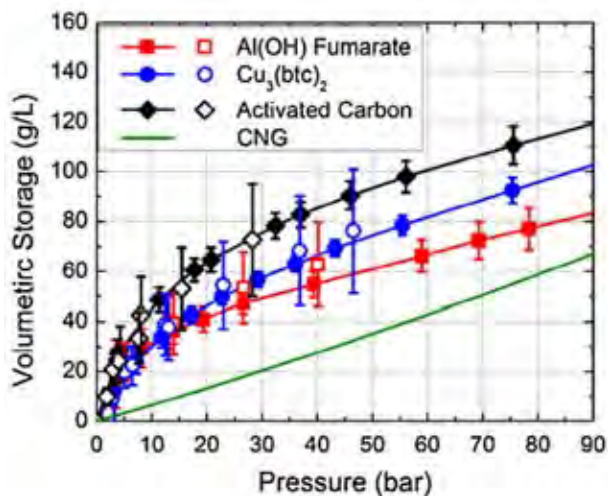
Figure 2.3   Comparison of volumetric storage between CNG and ANG technology (Beckner and Dailly, 2016).
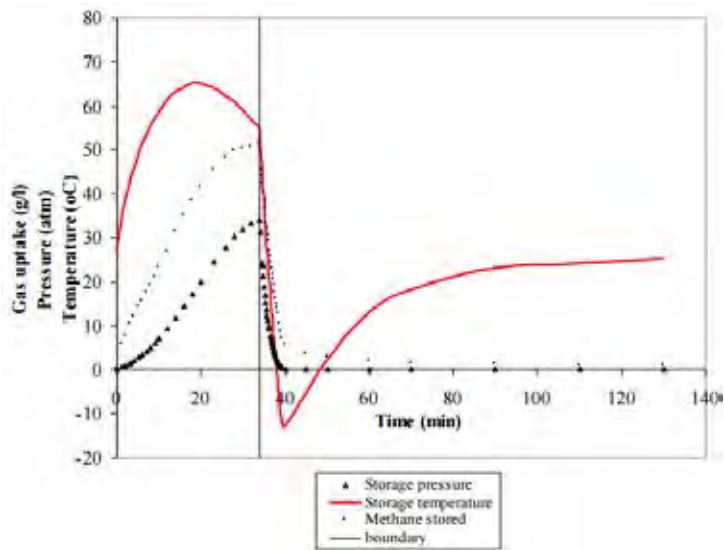
Figure 2.4 Charge and discharge profiles of the ANG storage with time (Zakaria and George, 2011).

2.4 Adsorption and Desorption

Adsorption is an ability of attraction between solid substances and molecules of gases or solutions, as shown in Figure 2.5. Gases molecule as adsorbate is adsorbed into solid materials namely adsorbent. They is collected in adsorbent by the external or internal surface of solid (walls of capillaries or crevices) or by liquid surface. Adsorption can be done by chemical or chemical adsorption. Physical adsorption look like the condensation of gases to liquids which is based on physical structure, or van der Waals force. Any gas can be adsorbed on any solid whenever the temperature is low enough or satisfactory by the pressure of the gas. In chemical adsorption, chemical forces hold gases and solid surface together that are specific for each couple of surface and gas. According to operating condition, the temperature of chemical adsorption usually is higher than physical adsorption. Moreover, chemical adsorption process takes time more than physical adsorption process (www.britannica.com). The reversible process of adsorption is desorption (Figure 2.6). This phenomenon is releasing gas adsorbed from adsorbent after equilibrium state of sorption between adsorbing surface and bulk phase (fluid, i.e. gas or liquid solution).

In addition, the adsorption process relates to the supplement of the gas density in the nearby of the contact surface. Because this is a spontaneous process, the Gibbs free energy change is lower than zero. Then, the entropy changes is also less than zero (a decrease in the freedom degree of the gas molecules during the process) and the enthalpy change is smaller than zero. From these condition, adsorption process is an exothermic reaction. On the other hand, desorption process is endothermic reaction (Solar *et al.*, 2010).

Adsorption and desorption isotherms depend on of the type, concentration and distribution of adsorption sites, pore structure of adsorbent, adsorptive and experimental conditions. In this work, the adsorption of methane and carbon dioxide on activated carbon and MOFs are studied. These adsorbents are two surface sites involving adsorption and desorption process. There are both hydrophobic and hydrophilic sites on carbon surfaces of adsorbents. Actually, gases are favourable adsorbed on polar adsorbate that adsorption starts on the polar sites (Fletcher *et al.*,

2006). Moreover, various studies have concluded that the features required by an adsorbent to be adequate for the ANG process are (Solar *et al.*, 2010):

a) High adsorption capacity.

b) High adsorption/desorption relations.

c) Micropore sizes of approximate 0.8 nm (bigger than the sizes of two molecules of methane) to facilitate the gas release at room temperature.

d) High packaging density to ensure that the storage capacity and the energetic density are high.

e) Low adsorption heat and high specific heat to minimize the temperature variation in the tank through the adsorption and desorption processes.

f) Suitable properties for the mass transference.

g) Being extremely hydrophobic.

h) Being inexpensive.
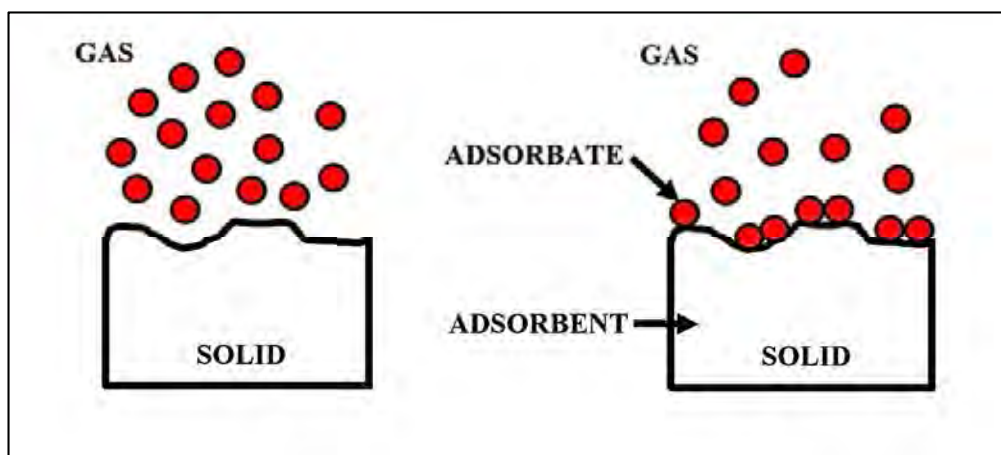
Figure 2.5 Representation of the adsorption processes of a gas on a solid surface for a given pressure and temperature (Solar *et al.*, 2010).
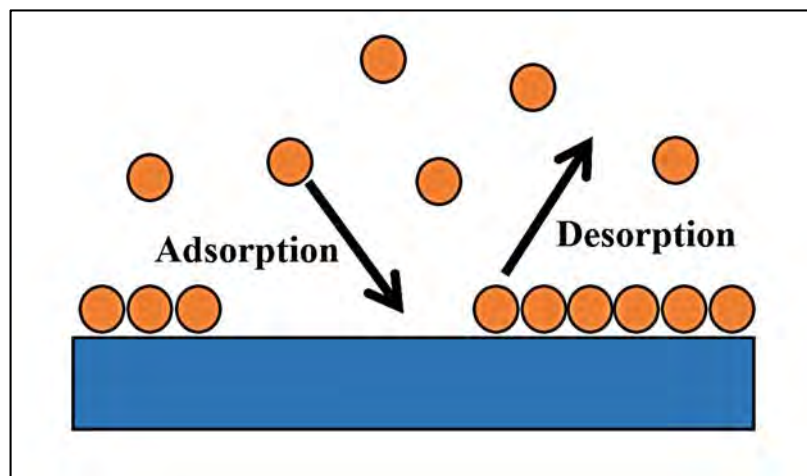
Figure 2.6 Adsorption and desorption process (www.emaze.com).

2.5 Adsorption Isotherms

Adsorption isotherms are critical in optimizing the use of adsorbents, and are important for the description of how adsorbate will interact with an adsorbent. It is usually described to determine the amount of adsorbate on the adsorbent as a function of its pressure (if adsorbent is gas) or concentration (if adsorbent is liquid) at constant temperature. In case of gas-solid adsorption, when a gas comes into contact with a solid surface, molecules of the gas will adsorb to the surface in quantities that are a function of their partial pressure in the solid. The measurement of the amount of gas adsorbed over a range of partial pressures at a single temperature results in a graph known as an adsorption isotherm. Adsorption isotherm in physical chemistry is generally expressed as concentration of adsorbed phase (or amount of gas adsorbed) per unit mass of adsorbent. It is a function of both pressure and temperature, besides the nature of the gas. The data may be represented as isotherms, V (P), at constant T, isobars, V (T) at constant P, or isosteres, P (T) at constant V. Among them, isotherms are the closest one to direct experiments. Measurements of pure component isotherms can easily be conducted and are generally available for adsorption design study. Meanwhile, the investigation of multi-component isotherms often hits a difficulty since the experimental data over design ranges of pressure, temperature, and

composition are impractically measurable. Therefore, many literature models are available to predict the mixture behaviors from pure component isotherm data (Jeong *et al.*, 2017).

2.5.1 IUPAC Classification of Adsorption Isotherm

Most analysis of adsorption equilibria begins with classification of the isotherms. This classification is important in theoretical modeling of adsorption phenomena. It also is important for practical reasons. As an illustration, consider surface area measurements using the BET method. There are international standards and a number of commercial devices for using this method in different applications. However, according to the IUPAC manual, the first step is to identify the isotherm type and hence the nature of the adsorption process. The modern version of IUPAC classification scheme is based on an earlier classification by Brunauer, which has five types of isotherms. It has six types of isotherms for gas/solid equilibria, as shown in Figure 2.7 (Donohue and Aranovich, 1998).

Type I isotherm approaches a limiting value and usually is used to describe adsorption on microporous adsorbents. Types II and III describe adsorption on macroporous adsorbents with strong and weak adsorbate-adsorbent interactions, respectively. Types IV and V are given by monolayer and multilayer adsorption plus capillary condensation. Type VI is not included in the Brunauer classification as it illustrates that the adsorption isotherms can have one or more steps (Donohue and Aranovich, 1998).

The classification of pores, according to their size, which is recommended by IUPAC, is described below (Solar *et al.*, 2010):

a) Pores with widths exceeding about 50 nm or 500 Å are called macropores.

b) Pores with widths not exceeding about 2 nm or 20 Å are called micropores.

c) Pores with widths between 2 nm (20 Å) and 50 nm (500 Å) are called mesopores.

However, the current IUPAC classification has two deficiencies: it is incomplete, and it gives the incorrect impression that adsorption isotherms are always

monotonic functions of pressure. Though not stated explicitly in the IUPAC publications, the IUPAC classification is limited to condensable vapors, but many important gas/solid systems fall outside this classification (for example, nitrogen, oxygen, fluorine, hydrogen, carbon dioxide, carbon monoxide, nitric oxide, methane, ethylene, and some freons at a room temperature). Moreover, this restriction is ambiguous because gases can be non-condensable in the bulk, but condensable in pores of an adsorbent. In 1999, Donohue and Aranovich presented a comprehensive analysis of adsorption behavior that is based on experimental results, molecular simulations, and lattice theory concepts proposed by Ono and Kondo in 1960. Figure 2.8 shows a new classification of adsorption isotherms. While general, the classification shown in Figure 2.8 is meant to be qualitative and does not show all possible details. In this classification (Donohue and Aranovich, 1998).

a) Type I shows adsorption isotherms on microporous adsorbents for subcritical, near critical and supercritical conditions. At supercritical conditions, the isotherm is not monotonic.

b) Types II and III give adsorption isotherms on macroporous adsorbents with strong and weak affinities, respectively. For low temperatures, these types have steps, but increasing temperature transforms them into the smooth monotonic curves, which are like those in Types II and III of the IUPAC classification. However, near the critical temperature, these isotherms change dramatically to non-monotonic behavior showing sharp maxima, and further increase in temperature leads to isotherms with smooth maxima.

c) Types IV and V characterize mesoporous adsorbents with strong and weak affinities, respectively. For lower temperatures, they show adsorption hysteresis. Supercritical isotherms for mesoporous adsorbents, which are predicted by lattice theory and the logic of this classification scheme, are also included.
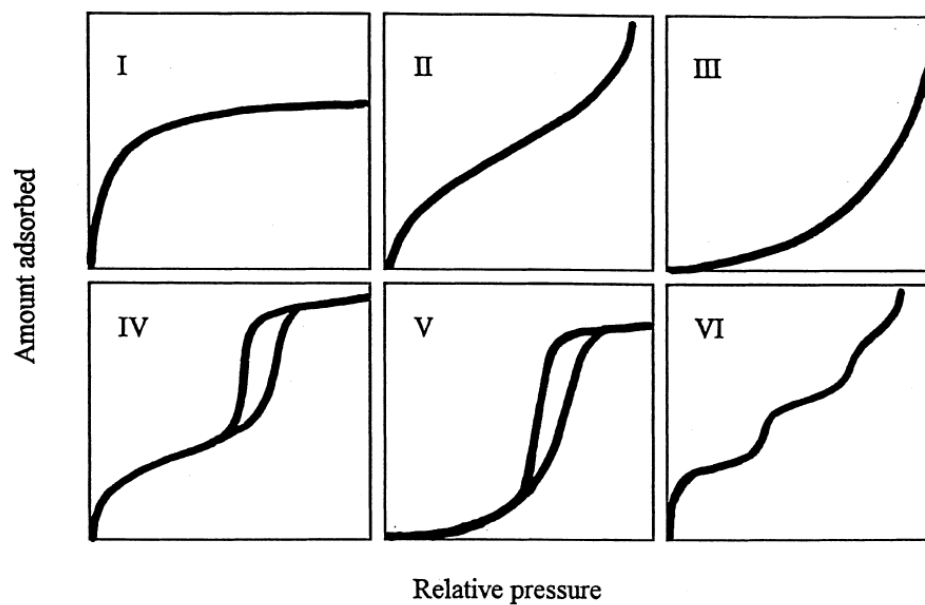
Figure 2.7 IUPAC classification of adsorption isotherms for gas/solid equilibrium (Donohue and Aranovich, 1998).
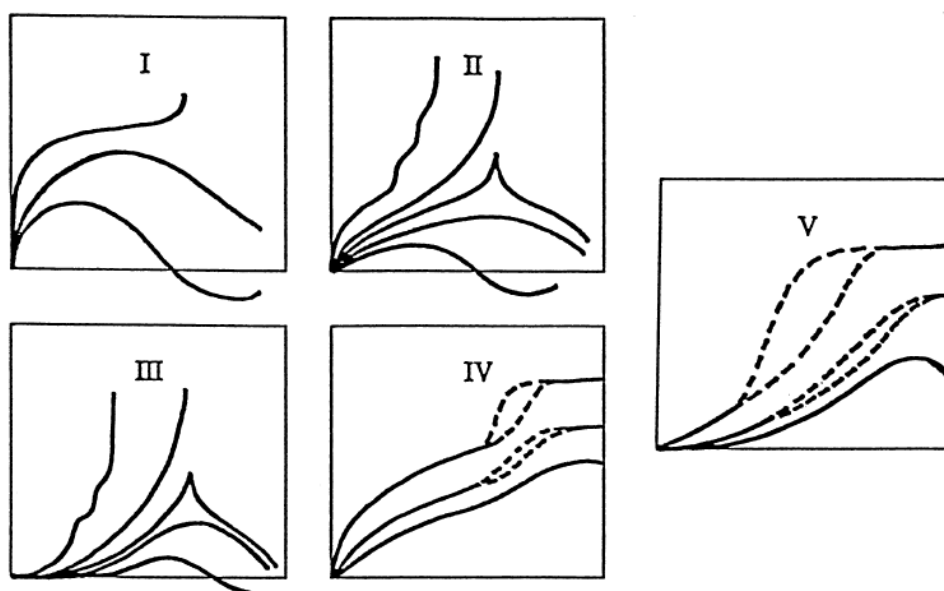
Figure 2.8 New classification of adsorption isotherms (Donohue and Aranovich, 1998).

2.5.2 <u>Measurement of Adsorption Isotherms</u>

Adsorption measurement is to determine the adsorption characteristics of adsorbent-adsorbate pair, including isotherm, kinetics, and heat of adsorption data. All these parameters are key variables for simulation and modeling of any adsorption process. Currently available adsorption measurement techniques or facilities can be basically classified into three types, i.e. volumetric, gravimetric, and gas flow (Kumar, 2011).

2.5.2.1 Gas flow technique

This approach, firstly proposed by Nelsen and Eggertsen, was a variant of gas chromatography. It used helium as carrier gas and a gas flow meter was used to determine the partial pressure of the adsorbate. The adsorbed volume was determined from the peak area in the adsorption/desorption chart recorded by a potentiometer over a period. This apparatus is simple, cheap and easy to handle, and no vacuum is required, and available gas chromatographers can be also modified for this approach. However, the measurement of the adsorbed amount is indirect and the method does not claim high accuracy. The method is usually applied for fast single point determinations of the specific surface area. Multipoint measurements of isotherms become complicated (Kumar, 2011).

2.5.2.2 Gas adsorption volumetric technique

In this technique, a given amount of adsorptive gas is expanded into a vessel, which includes a sorbent sample, and which initially has been evacuated upon expansion, the adsorptive gas is partly adsorbed on the (external and internal) surface of the sorbent material, partly remaining as gas phase around the sorbent. By a mass balance, the amount of gas being adsorbed can be calculated if the void volume of the sorbent, i.e. the volume, which cannot be penetrated by the adsorptive gas molecules, is known at least approximately. The line diagram of volumetric setup is shown in Figure 2.9 (Kumar, 2011).

2.5.2.3 Gravimetric method

In gravimetric method, the weight change of the adsorbent sample in the gravity field due to adsorption from the gas phase is recorded. Various types of sensitive microbalance have been developed for this purpose. A continuous-flow gravimetric technique coupled with wavelet rectification allows for higher

precision, especially in the near-critical region. The line diagram of gravimetric apparatus is shown in Figure 2.10 (Kumar, 2011).
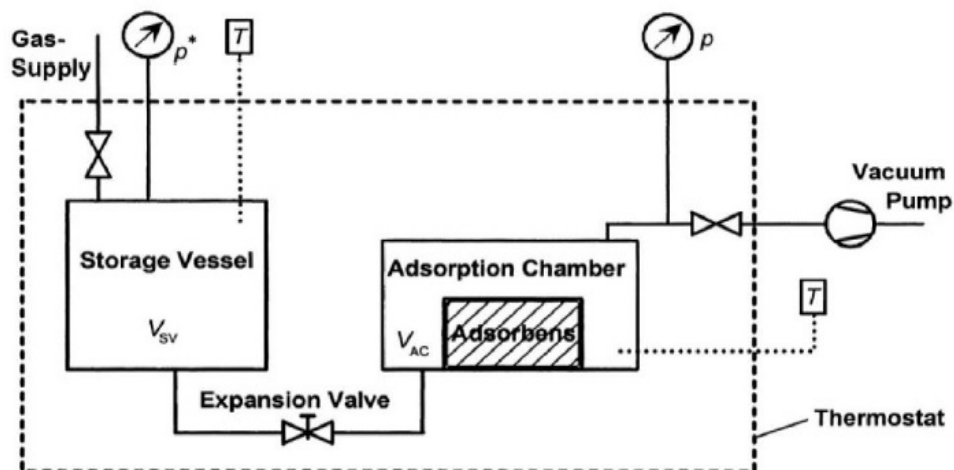
Figure 2.9 Experimental setup for volumetric measurement of pure gas adsorption equilibrium (Kumar, 2011).
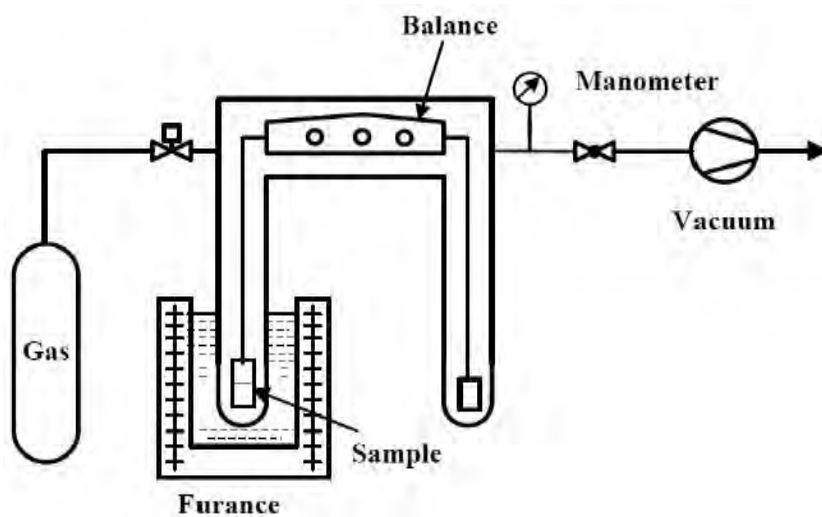
Figure 2.10 Schematic diagram of gravimetric apparatus (Kumar, 2011).

2.6 Adsorbents

The ideal adsorbents for natural gas storage are high microporous material with high packing density and limit macropores and micropores volume. The adsorption capacities performance is measure at standard condition, which is the volume of adsorbed natural gas per volume of storage (V/V). The highest experimental storage capacities achieved up to date (at 3.5 MPa and 25 °C) are for the high performance activated carbon.

The porous adsorbents that have been studied in the research for methane adsorption are normally microporous: zeolites, activated carbons, porous organic polymer networks, and metal-organic frameworks (MOFs) (Shen *et al*., 2015). Zeolites have limitation for methane adsorption because of their extremely hydrophilic, relatively low surface area (< 1,000 m^2/g) leading to low methane adsorption capacity. In this work, activated carbons and MOFs are studied (Li *et al*., 2016).

2.6.1 <u>Activated Carbon</u>

Porous carbon materials have been one of the most interested types of microporous materials for methane storage. The effect of micropore volume, pore size and shape and surface area were investigated in the researches. The major parameters of adsorbent for CH_4 adsorption are porous structure and pore morphology. Because methane are more favourable to fill in micropores than in macropores and mesopores, the amount of micropores need to be maximized (Bagheri and Abedi, 2011). Simulations and experimental studies have indicated that activated carbon with slit-shape pores 0.8-1.5 nm is the most suitable for methane storage. The more micropores lead to the greater amount of methane being adsorbed. However, there are some existence of the mesopores and macropores in structure. These types of micropores also play a part in the methane storage capacities because they allow pass through to the micropores with higher pressure then they improve filling micropores for higher methane uptake (Li *et al*., 2016). There are many advantages of activated carbon as adsorbent from their strong resistance to alkalis and acids, good hydrophobicity, and excellent thermal stability at relatively high temperature. In addition, van der Waals

forces is accepted to be an important role in adsorption of activated carbon (Bagheri and Abedi, 2011).

The major composition of activated carbon is carbon about 85-95% and the rest is hydrogen, nitrogen, oxygen, and sulfur (Arami-Niya *et al*., 2011). The proportion of each elements depends on the raw material and prepared process like activation and subsequence treatment. Raw materials for activated carbon can be prepared from different organic material with high carbon contents such as wood, coal, lignite, and some types of polymers by combustion, partial combustion, or thermal decomposition. Because the amount of activated carbon using increases then considering to the economical supplies are very importance. Thus, waste products from agriculture would be a good alternative in some applications because they can reduce disposed expenses and high carbon and low contents bring about to suitability as a precursors for activated carbon production, e.g. oil palm shell, coconut shell, pistachio shells, olive stones, etc. It is received that the pore structure and pore size distribution of AC influenced by various material composition, e.g. lignin, cellulose and halo-cellulose. Normally, specific surface area of widely used activated carbon varies from 800 to 1,500 m^2/g and pore volume varies from 0.20 to 0.60 cm^3/g. However, in some cases, the pore volume has been found to be as large as 1 cm^3/g (Bansal and Goyal, 2005).

Activation process for ACs have two methods (Arami-Niya *et al*., 2011).

a) Physical activation: this method of activation is in the gas phase. It is realized as thermal or physical activation. Firstly, hydrogen and oxygen contents are get rid of by pyrolysis of carbonaceous raw material at temperatures lower than 800 °C and inert atmosphere like argon or nitrogen. Then, chars are activated at temperature between 950 to 1,000 °C with oxidizer like steam and carbon dioxide. Thus, carbon atom are extracted from raw materials by endothermic reaction following these equations:

$$C + CO_2 \rightarrow 2CO \qquad \text{(Reaction 1.1)}$$
$$C + H_2O \rightarrow CO + H_2 \qquad \text{(Reaction 1.2)}$$
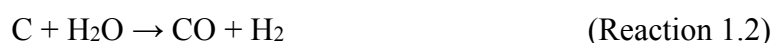
b) Chemical activation: this method involves the treatments of raw materials with a chemical agent prior to carbonization. The chemical is normally an

acid, strong base, or salt (phosphoric acid, sodium hydroxide, zinc chloride 25%). Then, conventional heat treatment is used at lower temperatures (450-900 °C) that dominates the carbonization process and causes the porosity. Actually, the process of carbonization of activation step is the same as chemical activation but operates at lower temperatures and takes less time for activating material.

c) Combination of chemical and physical activation: this method is another way to prepare activated carbon with high porosity. Arami-Niya *et al.* (2011) reveals that combination of two method can improve to get more homogeneous porosity than conventional method. In addition, pore size distribution can be adapted in this method.

Activated carbon has been obtained in three main forms; granular, pelletized, and powdered shown if Figure 2.11. Some materials are also prepared in spherical, fibrous, and cloth forms for some applications (Bansal and Goyal, 2005).

Figure 2.11 Pelleted, granular, and powder activated carbon (www.medaad.comz).

2.6.2 Metal Organic Frameworks (MOFs)

Nowadays, metal organic frameworks (MOFs) as a brand new class of microporous material have progressed extensive attention for the storage of methane at moderate pressure and room temperature. There has been rapid development of different MOFs for a long time because of their high porosity, diverse structure and designable.

MOFs are known as coordination polymers. It is basically a class of crystalline material, which composes of metal cation or cluster of cation and organic linker molecules connected together by coordination bonding as shown in Figure 2.12 Different metal ions, organic linkers can be combined to be several species of MOFs. MOFs can be designed with different geometries like tetrahedral, trigonal, bipyramidal square or pyramidal octahedral. As shown in Figure 2.13, metal ions are commonly Zn^{2+}, Al^{3+}, Ln^{3+}, Cu^{2+} and Cd^{2+}, et. Organic linkers such as sulfonates, carboxylates, nitrites, phosphates and amines also play a part in form of MOFs. Furthermore, coordination bonds have ability to rearrangement the construction of MOFs by reversible process throughout polymerization. Thus, MOFs can possess highly formed framework structure (Kumar *et al*., 2015).

Compared with activated carbon materials, they have higher mechanical strength that is benefit for avoiding packing-related loss of efficiency. So, this is excellent optimization for volumetric and gravimetric capacities, which is favourable for methane adsorption. On the other hand, activated carbon has some limitation for designing pore-size distribution. Surface area, surface functionalization and pore volume are also hardly accessible (Li *et al*., 2016). Actually, MOFs have high surface area and high micro-porosity but they emerge as an interested material because more functions could be adjusted such as porosity, topologies, open metal sites and framework densities solving some obstacles form conventional material (Shen *et al*., 2015).
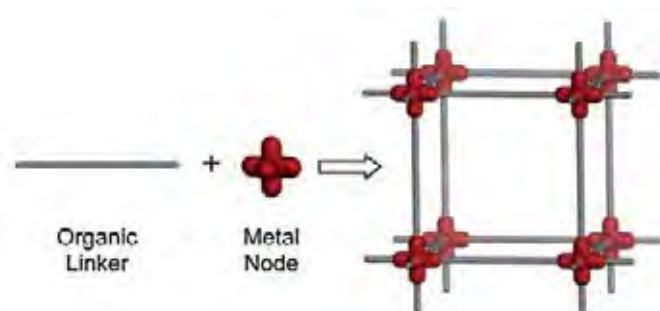
Figure 2.12 Simple framework connections of metal nodes and organic linkers for the construction of MOFs in a cubic topology (Kumar *et al*., 2015).
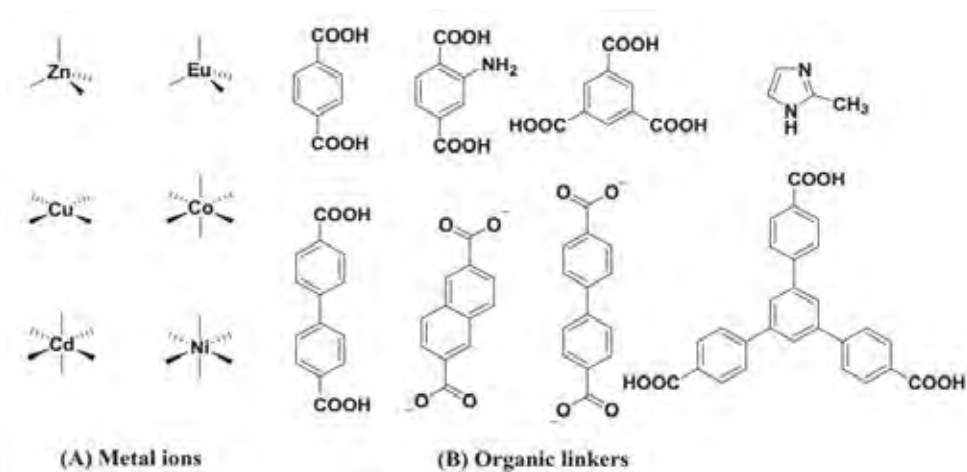
Figure 2.13 Example of the coordination geometry between (A) metal ions and (B) organic linkers used (in MOF synthesis) (Kumar *et al*., 2015).

A variety factors of MOFs such as open metal sites, framework densities, pore space, pore metrics (pore-size distribution) have been indicated to highly impact their methane storage performance. Several researches reveal that the total gravimetric methane storage is typically increased with increasing pore volume and surface area. Nevertheless, the high surface area of MOFs tend to have a low framework density that also reduces methane uptake. Thus, the optimization of pore spaces, porosities and framework densities need to be done (Li *et al*., 2016).

2.7 Literature Reviews

Adsorbed natural gas (ANG) is a technology to increase methane storage capacity by storing methane in highly microporous adsorbent at room temperature and modest pressure (3-4 MPa). This technology can compete with the CNG technology in many reasons. First of all, it is more comfortable condition from relatively low pressure. Energy requirement in compression process is lower, then single stage compressors are allowed. Thus, operating cost is reduced. Secondly, type of material used for storage methane is cheaper and storage tank is more suitable for vehicle because of lighter tank. However, high storage capacities of methane depend on characteristic in each adsorbents such as morphology, surface area, micropore volume, pore size distribution, operating condition and thermal effects. Hence, adsorption technology has been an interesting studies for researcher long time ago (Lozano-Castello et al., 2002).

Esteves *et al*. (2008) reported and analyzed experimental equilibrium data for single-component adsorption of CH_4, C_2H_6, C_3H_8, C_4H_{10}, CO_2 and N_2 on the activated carbon, which was measured by using a standard static gravimetric procedure. The reported data covered a wide range of thermodynamic conditions (0-90 MPa and 273-325 K). The single component adsorption isotherms of C_1-C_4, CO_2 and N_2 as shown in Figures 2.14 and 2.15. The shape of the adsorption isotherms is classified as Type I (monotonically concave isotherms) in the IUPAC classification. This result refers to characteristics of adsorbent as microporous material. These graphs also display reduction of adsorption when the temperature increases due to exothermic process of physical adsorption.
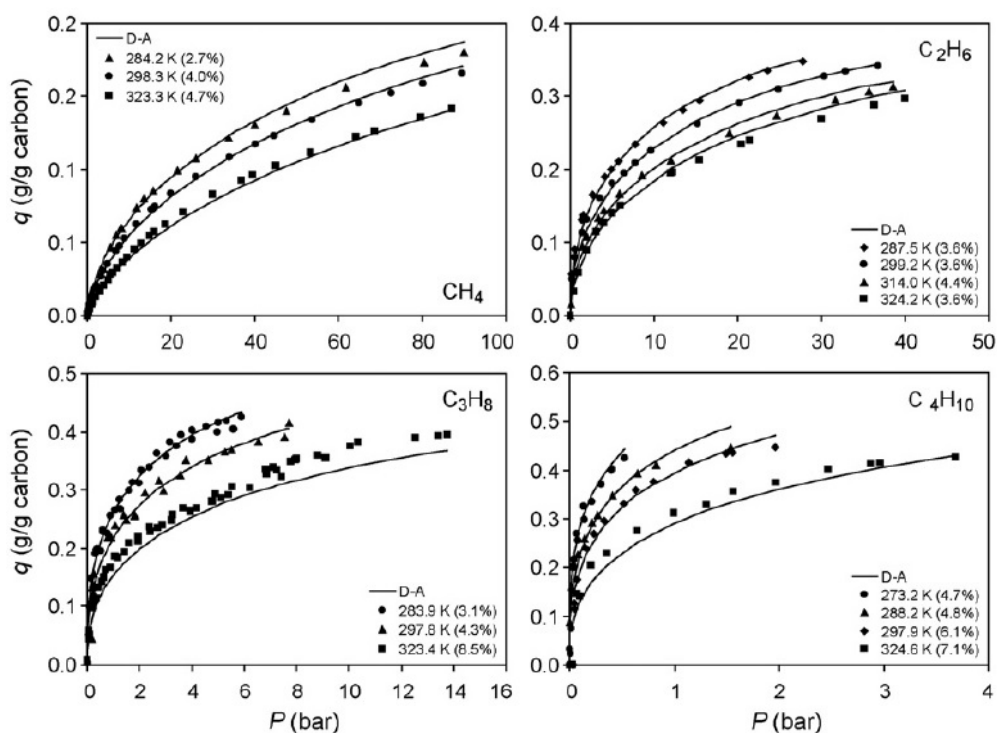
Figure 2.14 Single-component adsorption isotherms for the n-alkanes C_1-C_4 (Esteves *et al.*, 2008).
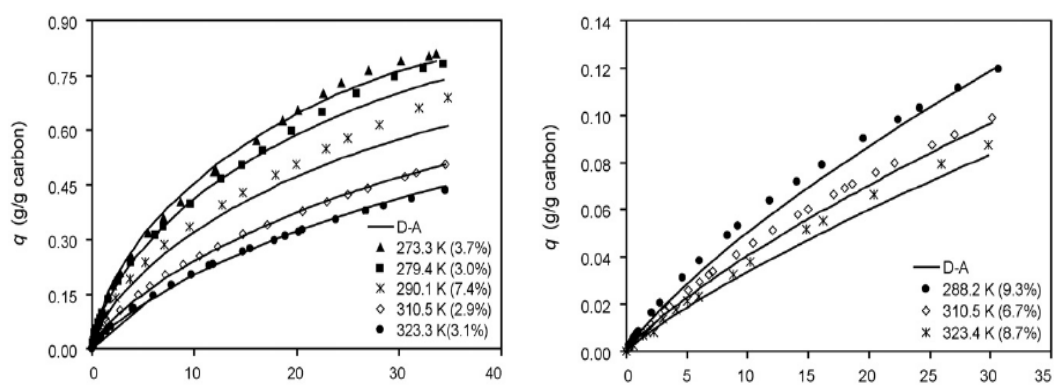
Figure 2.15 Single-component adsorption isotherms for CO_2 (left) and N_2 (right) (Esteves *et al.*, 2008).
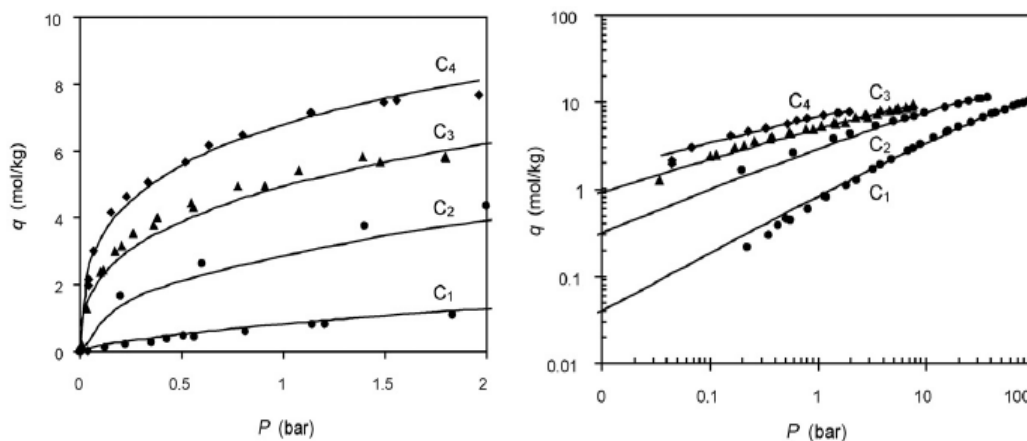
Figure 2.16 Comparative of adsorption isotherms for the n-alkanes C_1-C_4 at 298 K (Esteves *et al.*, 2008).

Figure 2.16 compares the single-component adsorption isotherms for the C_1-C_4 alkanes at 298 K. The left graph is an expansion of the low-pressure region that adsorption isotherm strongly increases with hydrocarbon chain length. However, the full pressure region on a log-log scale shows the inverse trend to the left graph. Therefore, desorption of higher molecular weight are not favourable when a downwards pressure swing of carbon is happened. This is an inconvenient from accumulation of heavy hydrocarbon that blocks methane delivering to engine during cyclic operation (Esteves *et al.*, 2008).

Nanoporous carbons were analyzed for methane and carbon dioxide adsorption isotherm and adsorption enthalpies at room temperature and up to 25 bar. The porous carbon was synthesized from mixing pyrogallol-formaldehyde with water and used $HClO_4$ as catalyst. This adsorbent was pyrolyzed at 1,000 ºC. Adsorption isotherm of carbon dioxide and methane are illustrated in Figure 2.17(a). It can be seen that the adsorption capacity of carbon dioxide is higher than methane and same trend as heat of adsorption (ΔH_{ads}) shown in Figure 2.17(b) indicating comparatively higher adsorbent-adsorbated interaction. The reason is quadrupole moment (-14×10^{-40} C m^2) of carbon dioxide, which induces specific interactions with adsorbents while methane has not. Moreover, the experimental condition also affects to adsorption of methane and carbon dioxide. The adsorption at 302 K is nearly to the triple point temperature

of carbon dioxide than methane In this condition, methane is supercritical gas (T_c (CH_4) = 190.53 K) while the critical temperature of carbon dioxide (304.21 K) is slightly higher than experimental temperature (Djeridi *et al.*, 2017).

Bagheri and Abedi (2011) studied methane adsorption capacities on various corn cob based activated carbon at different pressures (500, 1000, 1500 and 2000 psi) and different temperatures (298 and 323 K) in a volumetric adsorption apparatus. Six activated carbons were prepared at different conditions with various BET specific surface areas. Gravimetric equipment were used in this experiments.
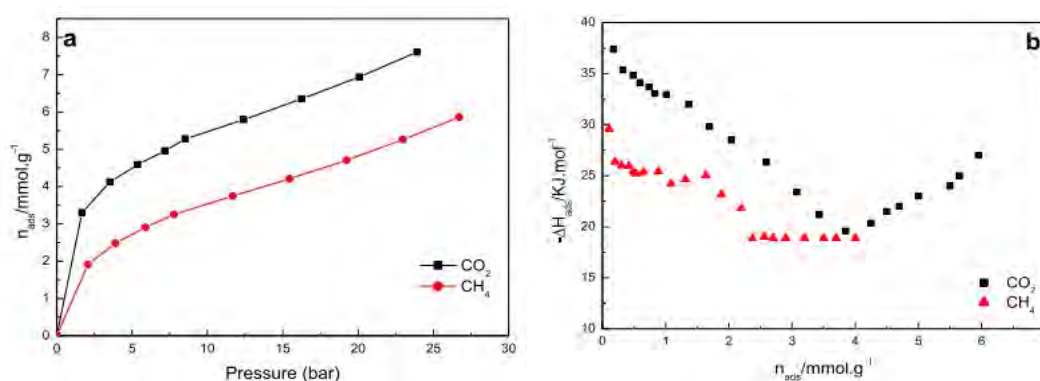
Figure 2.17 Adsorption isotherms (a) and adsorption enthalpy (b) of CO_2 and CH_4 at 302 K on the nanoporous carbon based on pyrogallol-formaldehyde (Djeridi *et al.*, 2017).
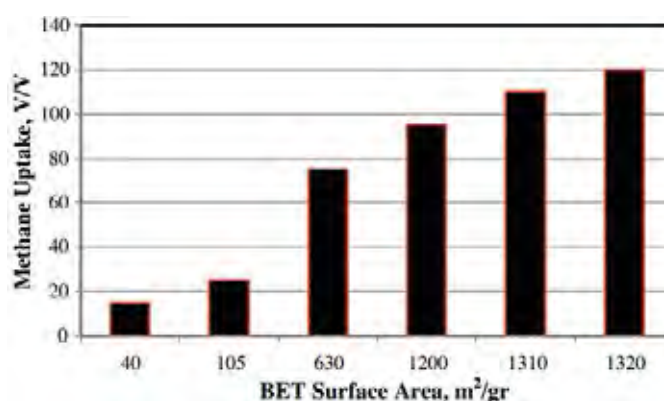
Figure 2.18 Variation of methane adsorption capacity with BET surface area, at a pressure of 500 psi and temperature of 298 K (Bagheri and Abedi, 2011).

Figure 2.18 shows that natural gas adsorption increases with increasing of BET specific surface area because the higher BET specific surface area means there are more micropores which effectively increases the adsorption of natural gas. Micropores that are less than two or three molecular diameters in width of methane are very important. Thus, mesopore and macropore which pores size larger than 2 nm affect to adsorption capacities of methane by decreasing methane storage even though they are also beneficial for pass through methane between micropore and larger pore with different pressure (Bagheri and Abedi, 2011).

The best sample with a high BET surface area and a high adsorption natural gas capacity was chosen to investigate the effect of pressure and temperature on adsorption capacity. Figure 2.19 shows gravimetric and volumetric capacities of sample with different pressures at 298 K . The amount of methane adsorption increases when the pressure increases from 500 to 1500 psi as a result from increasing of the van der Waals attraction forces between the gas and adsorbent molecules. On the other hand, when the pressure increases over 1500 psi, the methane adsorption capacities decreases since it may be the saturation of the adsorbent or over pressure lead to destruction of micropores (Bagheri and Abedi, 2011).
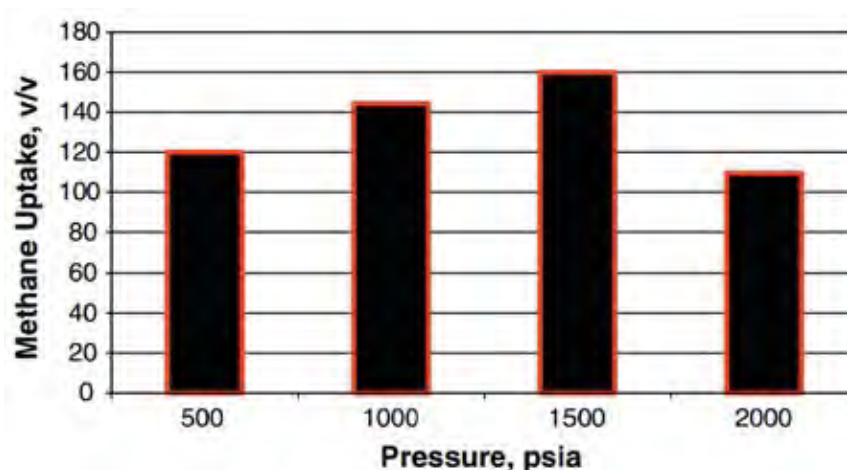
Figure 2.19 Variation of methane adsorption capacity with pressure at a temperature of 298 K (Bagheri and Abedi, 2011).
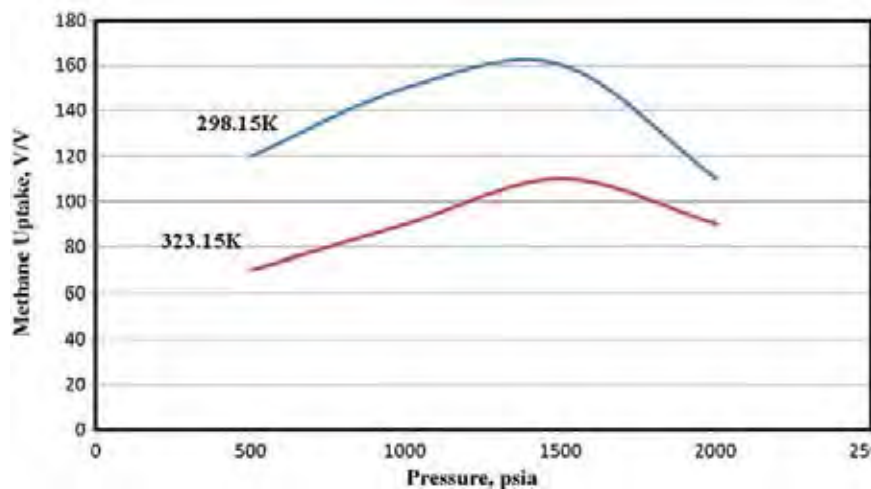
Figure 2.20 Variation of methane adsorption capacity with pressure at two different temperatures (Bagheri and Abedi, 2011).

Figure 2.20 presents the methane adsorption at various pressures and two different temperatures that lower temperature condition bring about to reduce methane storage due to exothermic process of adsorption (Bagheri and Abedi, 2011).

In Zakaria and George (2011) report, the commercial grade palm shell-derived activated carbon adsorbent was used to test performance for ANG storage system under different gas charging and discharging rate. This work was examed with pressurization from atmospheric pressure to 3.5 MPa and its gas delivery performance by depressurizing to back atmospheric pressure. Palm shell activated carbon was in granular form.

As illustrated in Figure 2.21, the rising temperature from initial condition of the lower charging rate is lower than the higher charging rate. The condition that greater temperature rise takes place at faster charging rate is due to the exothermic adsorption reaction and to the adsorbent low thermal conductivity that leads to poor heat dissipation, especially for activated carbon adsorbents. Since gas adsorption is inversely proportional with temperature, the temperature increasing during charging leads to greater amount of heat of adsorption is generated per mole of gas charged into the vessel and the lower storage capacity is obtainable. In a similar way, the extent of cooling during discharge at different flow rates influence gas delivery capacity from

the ANG storage. As shown in Figure 2.22, the slower the discharge rate, the lower the temperature dropping after finishing adsorption. Likewise, faster gas flow rate during discharge leads to lower delivery capacity. When temperature and pressure drop occur during desorption, bearing in mind that lower temperature promotes adsorption, consequently part of the gas molecules tends to remain within the adsorbent micropores as the temperature falls. As a result, the amount of gas delivered from the ANG storage decreases and the percentage of this delivery capacity loss get higher when greater temperature drop takes place (Zakaria and George, 2011).
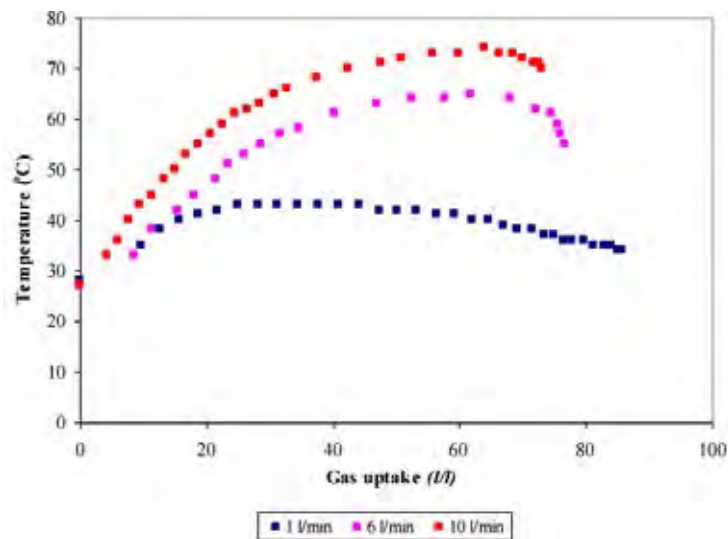
Figure 2.21 Effect of charging rate on gas uptake with temperature (Zakaria and George, 2011).
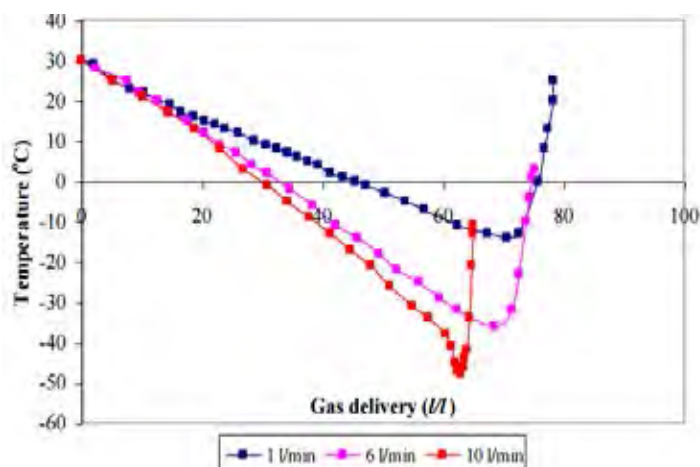
Figure 2.22 Effect of discharging rate on gas delivery with temperature (Zakaria and George, 2011).

Several activated carbons pellets without binder from the olives stones at various activation temperatures were investigated (Djeridi *et al.*, 2013). Preparation of activated carbon was done by using olive stones with phosphoric acid (H_3PO_4) by chemical activation. Varying from 350-1,000 °C is the activation temperature. Adsorption of N_2 (-196 °C) and SEM were used to characterize all carbons. The amount of methane storage associated with the micropore volume and specific surface area, delivered by the adsorption of N_2 at -196 °C. The effect of texture and also activation temperature on the adsorption of methane were the major interesting for them. They found that adsorbent with activation and pyrolysis by inert gas (N_2) contributed to increase in the porosity. This increment is probably because of the removal of volatile matters constructed during pyrolysis and discharge of the surface for creation of the new pores in the carbon structure. As concluded in Table 2.2, it presents specific surface area ranging from 532 to 1,014 m^2/g, micropore volume varied from 0.290 to 0.468 cm^3/g and pore size distribution varied from 1.79 to 1.95 nm.

Table 2.2 Pore properties of activated carbon pellets from olive stones and methane adsorption capacity at 23 bar and room temperature (Djeridi *et al.*, 2013)

Sample	BET (m^3/g)	V_{micro} (cm^3/g)	d_p (nm)
ACP350	826	0.381	1.91
ACP410	1014	0.468	1.85
ACP470	765	0.357	1.86
ACP500	700	0.342	1.95
ACP600	632	0.290	1.83
ACP800	532	0.249	1.87
ACP1000	915	0.404	1.79

It can be noticed in Figure 2.23 that CH_4 adsorption capacity trend grows up with increasing of micropore volume. Nevertheless, there are some exceptions in this trend that even though ACP600 sample and ACP800 sample have micropore volume less than ACP350 sample and ACP500 samples respectively but CH_4 adsorption of ACP350 sample is greater than ACP600 sample and also CH_4 adsorption of ACP500 sample is greater than ACP800 sample. The reason is due to the amount of CH_4 adsorption not only depends on micropore volume but also relates to the pore size distribution. As you can see that ACP600 sample and ACP800 sample have pore size distribution higher than ACP350 sample and ACP500 samples respectively as shown in Table 2.2. Thus, the lower the pore size distribution, the higher the amount of CH_4 being adsorbed. From these result, when the pyrolysis temperature changes, it affects to the BET surface area, the micropore volume, and also pore size distribution relating on CH_4 storage (Djeridi *et al.*, 2013).
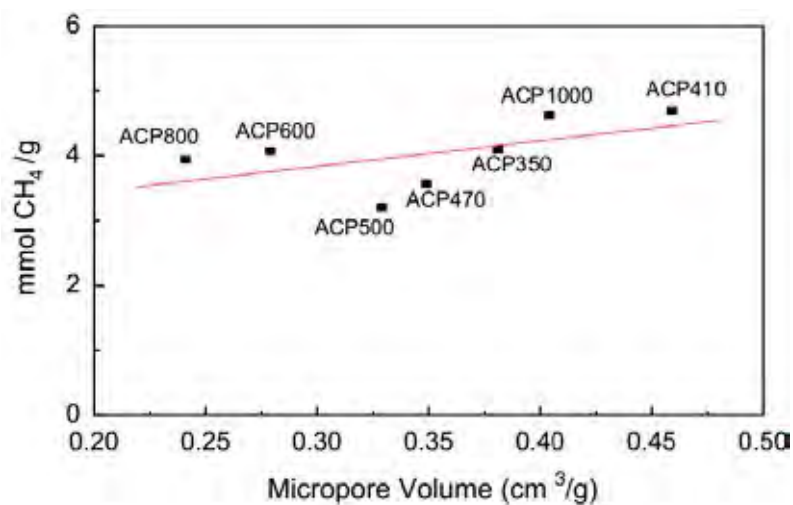
Figure 2.23 Relationship between the CH_4 adsorption capacity at 23 bar and room temperature with the micropore volume calculated from N_2 adsorption isotherms (Djeridi *et al.*, 2013).

As an experimental data from Teo *et al.* (2017), they studied methane storage on HKUST-1 and MIL-101 (Cr) metal organic framework (MOFs) at the temperature varying from 303 K to 343 K and pressure up to 600 kPa. From X-ray diffraction, it shows that HKUST-1is the microporous material with a good number of tiny pores or cavities, while it indicates that MIL-101(Cr) has abundant pores. They found that the structural of MOFs was responsible for more CH_4 or CO_2 uptakes. Two types of strong adsorption sites were observed in MOFs namely the open metal coordination sites with Coulomb attraction and van der Waals potential pore sites with dispersive interactions. The results suggested that the development of novel MOFs should focus on enriching open metal sites and minimizing the fraction of large pores.

Diffusion of pure methane, ethane, propane, n-butane, and binary mixture of methane with other hydrocarbon within micropores of several metal-organic frameworks (MOFs) were studied in Borah *et al.* (2015) research. Materials with varying topologies are the MOFs PCN-14, NU-125, NU-1100 and DUT-49. Firstly, diffusion coefficient of pure components was observed. The diffusion coefficients followed the order methane, ethane, propane and butane. Methane diffused fastest in all of these MOFs due to its low mass and smaller size, whereas diffusion coefficients

decreased as the chain length was increased due to the increase in the mass and size. Moreover, they investigated the effect of presence of the impurities, ethane, propane, and butane, on the diffusion of methane. Figure 2.24 presents that there are some minor increases or decreases due to the presence of methane, but the effects are insignificant. They suggested that the longer alkanes do not block the diffusion path of methane in any of the MOFs studied.

The comparison of methane storage in activated carbon and two metal-organic frameworks ($Cu_3(btc)_2$ and $Al(OH)$ Fumarate) was studied. These adsorbents represent a diverse variety of pore structures and surface chemistries. All materials were in powdered form. The excess adsorption, skeletal density, bulk density, and porosity were considered. Volumetric storage capacities are effected by excess adsorption, skeleton density and bulk density but the bulk density is also influenced by inter-granular porosity and intra-granular porosity. Because the skeletal density and excess adsorption are specific properties of the material and are steady with moderate compaction of the powder. Thus, the volumetric storage capacities can be improved by increasing the bulk density. From Figure 2.25, it is a decomposition of the volumetric storage with pressure of different materials. The green line is overall methane density that increases with increasing pressure. At low pressure, the volumetric storage capacity is dominated by excess adsorption. When the pressure increases, the excess adsorption get to the maximum and finally the volumetric storage density is dominated by the contribution from the inter-granular or intra-granular porosity (Beckner and Dailly, 2016).
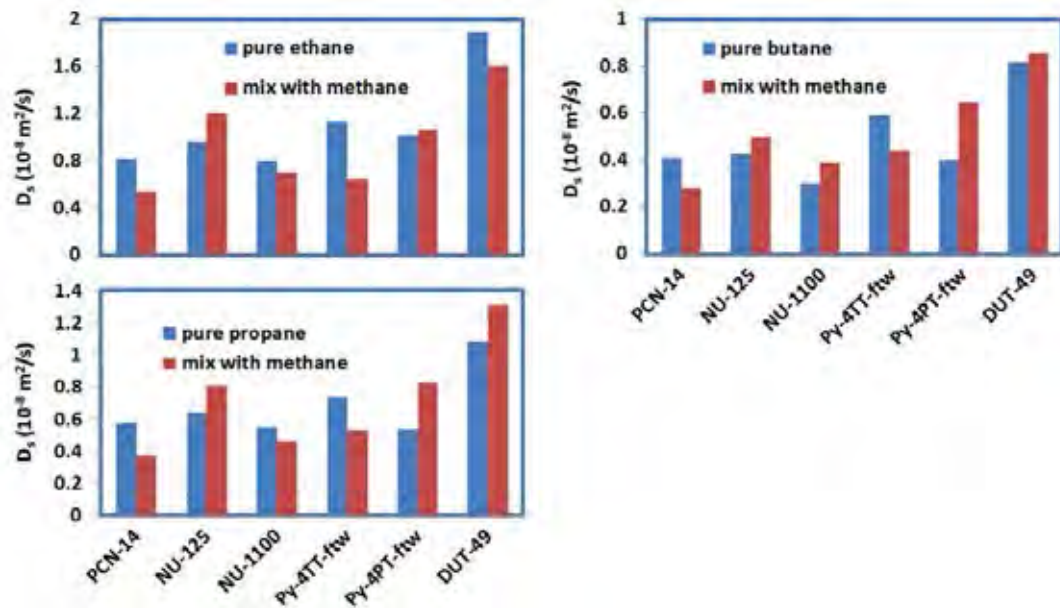
Figure 2.24 Comparison of diffusivities of the impurity components when they are pure and when they are in mixtures with methane (Borah *et al.*, 2015).
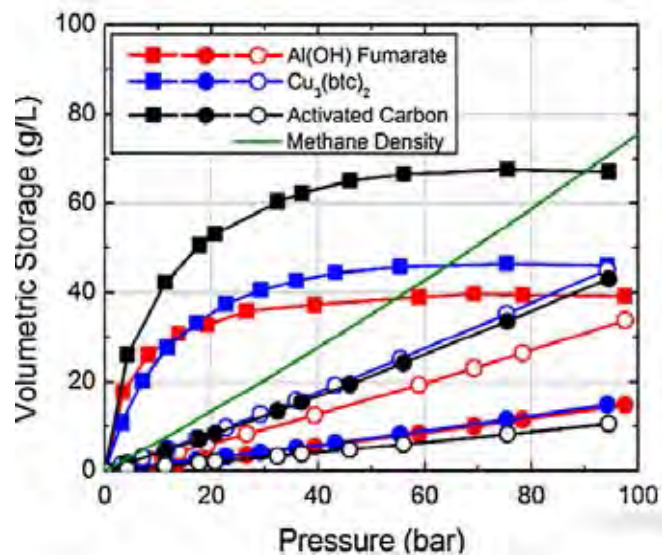
Figure 2.25 A decomposition of the volumetric storage for comparing the relative contributions of the excess adsorption (solid square), the intra-granular porosity (solid circles), and the inter-granular porosity (open circles) (Beckner and Dailly, 2016).

Table 2.3 Density and porosity measurements summary (Beckner and Dailly, 2016)

Property	Activated Carbon	Al(OH) Fumurate	$Cu_3(btc)_2$
Skeletal density (g/cm^3)	2.2	1.7	2.5
Bulk density (g/cm^3)	0.54	0.57	0.37
Intra-granular pore volume (cm^3/g)	1.13	0.35	0.57
Inter-granular porosity	0.15	0.46	0.64
Intra-granular porosity	0.61	0.20	0.21

Since bulk density and skeletal density result in a volumetric storage, adsorbent with high bulk density and high skeletal density lead to high volumetric storage. Therefore, activated carbon was expected to be the highest volumetric storage because of high bulk density and high skeletal density from their experiments while Al(OH) Fumulate is only high for bulk density, and $Cu_3(btc)_2$ is only high for skeletal density as shown in Table 2.3. However, when they consider for improving the bulk density. The inter-granular porosity becomes important. The larger inter-granular porosity, the better bulk density can be modified than the based material. The upper limit to the bulk density presents that inter-granular porosity becomes zero and intra-granular porosity becomes larger from densification. From their experiments, it shows that both MOFs have a much larger inter-granular porosity (0.5) than the AC (0.15) indicating that they can be most modified by densification (Beckner and Dailly, 2016).

From Figure 2.26, little change can be seen for the AC, which has the smallest undensified inter-granular porosity. For the Al(OH) Fumarate, there is also only a small change upon maximum densification. This is mostly because Al(OH) Fumurate has a small pore volume. Thus, even though adsorbent is high inter-granular porosity, improvement of bulk density is limited by small pore volume. The $Cu_3(btc)_2$ becomes the most promising for densification. The maximally densified material is approximate to be able to store nearly twice the methane at 50 bar than the undensified material (Beckner and Dailly, 2016).
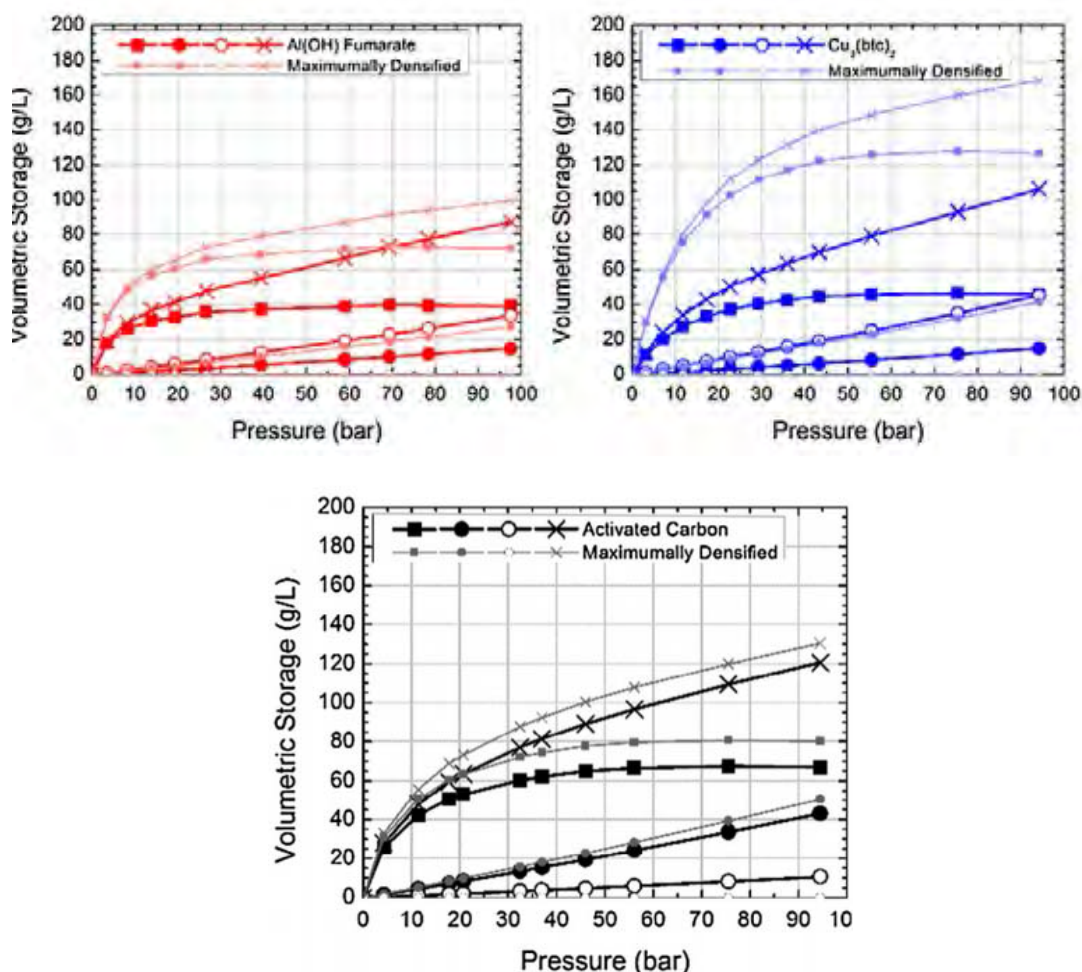
Figure 2.26 A comparison of the contributions to the total volumetric storage (X symbols) from the excess adsorption (square symbols), intra-granular porosity (solid circles), and inter-granular porosity (open cycles) for the maximally densified materials (Beckner and Dailly, 2016).

Himeno *et al*. (2005) studied the high pressure adsorption equilibrium of CH_4 and CO_2 on commercial activated carbons, made from coal (BPL), chark (Maxsorb), petroleum pitch (A10 fiber), and coconut shell (Activated carbon A). The adsorption isotherms of CH_4 and CO_2 onto activated carbons were obtained for temperatures from 273 to 333 K and pressures up to 6 MPa. Figure 2.27 shows the adsorption isotherms of CH_4 and CO_2 on activated carbons by the gravimetric method. From all of activated carbon, the amount of CH_4 adsorbed was less than two times of CO_2 adsorbed.

Maxsorb adsorbed was the highest among all of adsorbent being tested. It proved that BET surface area and pore volume dominate the amount CH_4 and CO_2 uptake. The higher the BET surface area and pore volume are, the greater the amount of adsorption is. The adsorption capacity Maxsorb is more than Activated carbon A, A10 and BPL respectively.
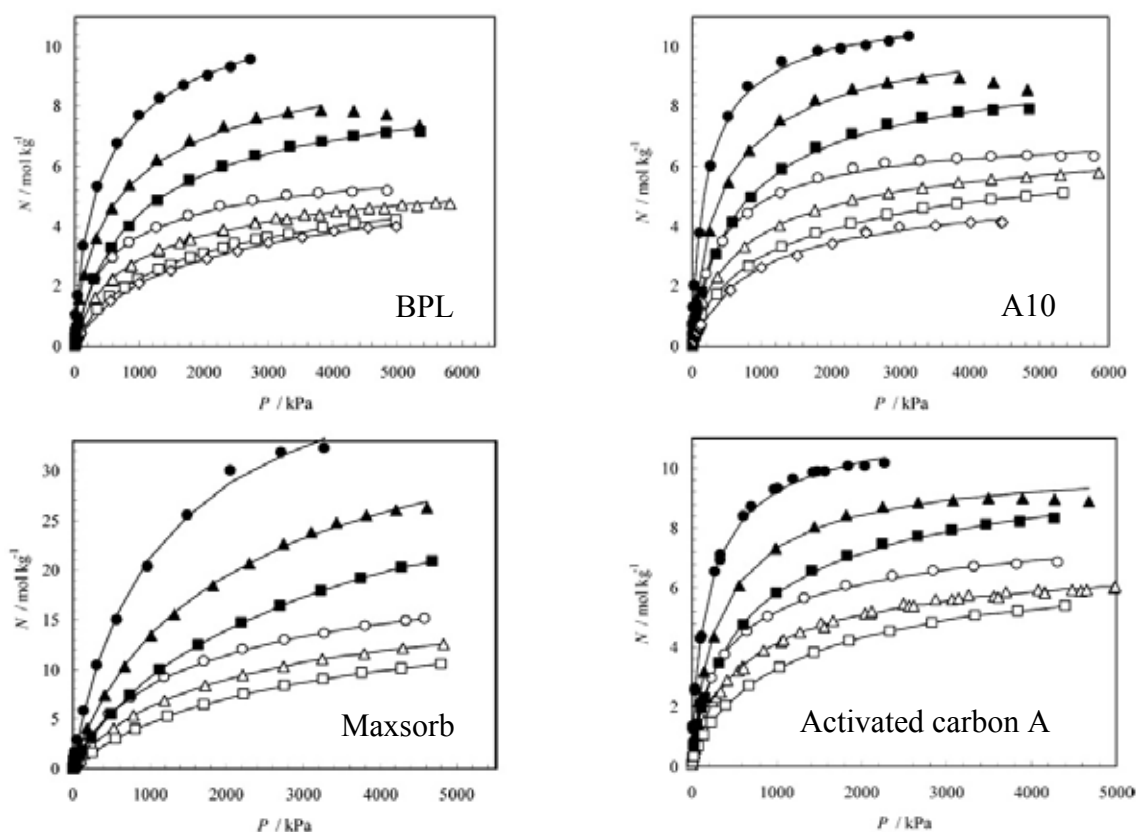
Figure 2.27 Adsorption isotherms of CH_4 and CO_2 on activated carbon: O, CH_4 at 273 K; △, CH_4 at 298 K; □, CH_4 at 323 K; ●, CO_2 at 273 K; ▲, CO_2 at 298 K; ■, CO_2 at 323 K (Himeno *et al.*, 2005).

CHAPTER III
EXPERIMENTAL

3.1 Materials and Equipment

3.1.1 <u>Materials</u>

- Fittings and valves
- Mass flow controller
- Vacuum pump
- Data logger
- Thermometer
- Activated carbon (AC), ZIF-8, UiO-66, and MIL-53 (Al) (supported by NANOTEC, Thailand)
- 50 wt% AC and 25 wt% AC (The percent in front of AC indicates the amount of AC mixed with PVDF) (supported by NANOTEC, Thailand)
- 75 wt% ZIF-8, 50 wt% ZIF-8, and 25 wt% ZIF-8, (The percent in front of ZIF-8 indicates the amount of ZIF-8 mixed with PVDF) (supported by NANOTEC, Thailand)
- Methane gas (99.99% purity purchased from Labgaz Thailand Co., Ltd.)
- Carbon dioxide gas (99.99% purity purchased from Labgaz Thailand Co., Ltd.)
- Helium gas (99.99% purity purchased from Praxair Inc., Thailand)

3.1.2 <u>Equipment</u>

1. Volumetric apparatus
2. Fourier transform infrared spectroscope (FTIR), Nicolet/Nexus 670
3. Scanning electron microscope (SEM), Hitachi S-4800

4. Surface area analyzer (SAA), Quantachrom/Autosorb1-MP
5. X-ray diffraction (XRD)

3.2 Experimental Procedures

3.2.1 Adsorbent Preparation

a. Activated carbon, 50 wt% AC, 25 wt% AC, ZIF-8, 75%ZIF-8, 50 wt% ZIF-8, 25 wt% ZIF-8, UiO-66, and MIL-53 (Al) were dried at 120 °C for 24 hours to remove moisture.

b. Keep in a desiccator.

3.2.2 Adsorbent Characterization

a. The surface area, total pore volume, and pore size distribution of the adsorbents was measured by a Quantachrom/Autosorb1-MP instrument. The adsorbents were first out gassed to remove the humidity on its surface under vacuum at 300 °C for 16 hours prior to the analysis. After that, nitrogen was purged to adsorb on its surface. The volume-pressure data was used to calculate the BET surface area, total pore volume, and pore size distribution.

b. The morphology of the adsorbents was investigated by using the SEM, Hitachi S-4800, with an accelerating voltage of 2 kV The adsorbents were coated with platinum under vacuum condition before observation.

c. Fourier transform infrared spectroscopy (FTIR) was used to qualitatively evaluate the chemical structure of the adsorbents. The IR spectra was collected using a Nicolet, Nexus 670 FTIR spectrometer. The adsorbent samples were grounded into fine powder and mixed with KBr. The mixture was used for the preparation of KBr pellets. The IR spectrum was obtained over a frequency between 400 and 4,000 cm^{-1}.

d. X-ray diffraction was used to confirm the crystalline structure of metal organic frameworks. It were carried out with a diffractometer

Bruker D8 Advance using Cu radiation (scan range 5 ° to 45 °), supported by NANOTEC, Thailand.

3.3 Adsorption Measurement

The schematic of the experimental set-up is shown in Figure 3.1. A pressure transmitter was installed to measure pressure of the system. One gram of the prepared adsorbent was loaded into the stainless steel adsorption chamber, which was heated by the furnace in order to reach the adsorption temperatures. He (Ultra high purity, Praxair Inc.) was used as a purge gas in this study. The adsorption processes were carried out using high purity CO_2 gas (99.99%). Effects of adsorption temperature were investigated by heating up to the temperature at room temperature, 35 °C within a pressure range of 0-100 psia. The temperature of the adsorption chamber was adjusted and maintained by an internal temperature sensor.
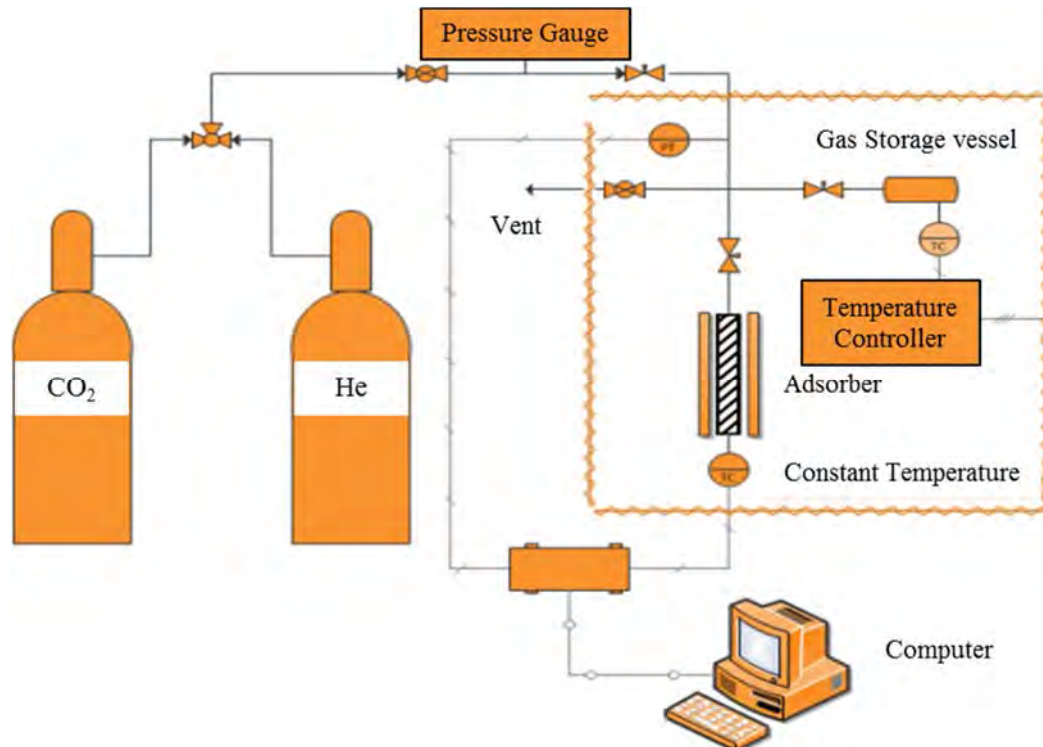
Figure 3.1 Schematic of the experimental set-up for the equilibrium adsorption of CO_2.

The volumetric apparatus was used to study methane adsorption on activated carbons. This apparatus consisted of a sample holder, a vacuum pump, and pressure transducer. Ultra-high purity grade methane (99.99 % purity) was used in the adsorption study. The schematic diagram of volumetric apparatus for this research is shown in Figure 3.2

A gas reservoir was a high pressure stainless steel reactor, and the pressure regulator with 4,000 psig maximum limit was installed to control a gas flow rate into the system. A K-type thermocouple was used for measuring the temperature of gas inside the reactor. The system pressure was measure by pressure transducer in the range of 0 to 3,000 psig with 0.13% error.

For each experiment, about 1.0 g of adsorbents was weighed and put into the sample holder. Next, the adsorbents were degassed by using a rotary vacuum pump prior to the methane adsorption. The temperature was controlled at room temperature (35 °C) within a pressure range of 0-100 psia. The pressures of gas were recorded before and after each gas expansion.
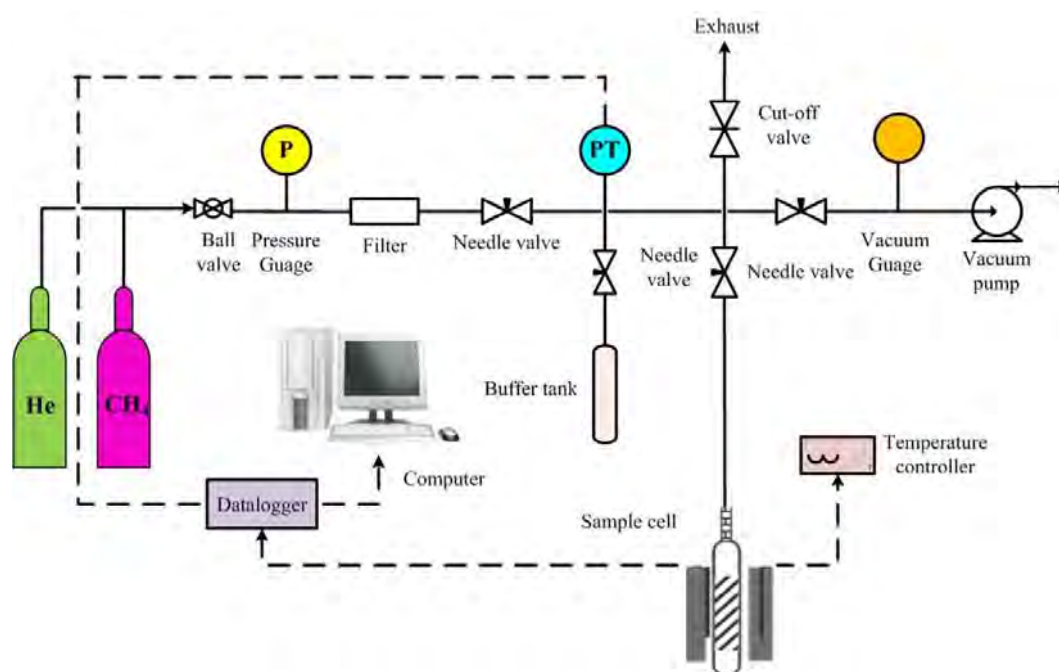
Figure 3.2 Schematic of the experimental set-up for the equilibrium adsorption of CH$_4$.

3.4 Adsorption Calculations

The amount of pure methane and carbon dioxide adsorption was determined by using Eq. (3.1).

$$n_i = \frac{1}{W} \left(\frac{P_1(V_1+V_2)}{ZRT} - \frac{P_2(V_1+V_2)}{ZRT} \right)$$

(3.1)

Where n_i = Mole of adsorbed CH_4 and CO_2 (mole)

P_1 = Pressure of the system before equilibrium (atm)

P_2 = Pressure of the system after equilibrium (atm)

V_1 = Volume of a manifold (cm^3)

V_2 = Volume of a cylinder with adsorbent (cm^3)

Z = Compressibility factor

R = 82.05 (cm^3atm/moleK)

T = Temperature of the sample (K)

W = Weight of adsorbent (g)

The pressure transducer was calibrated for every adsorption experiment. The vacuum pressure of -14.7 psi was used as the reference pressure. With this pressure, the relative was set to zero under vacuum condition.

1. Determination of the sample holder volume using helium

The volume of the sample holder was determined by helium expansion at 30°C, based on the assumption that no helium was adsorbed on the adsorbents. The pressures before and after each helium expansion were recorded.

To calculate the volume of instrument after helium expansion, V_2, Ideal Gas Law was used as followed.

$$\frac{P_1V_1}{T_1} = \frac{P_2V_2}{T_2}$$

(3.2)

Where   P$_1$ =   Pressure of helium before helium expansion

V$_1$ =   Volume of the system excluding volume of sample holder

T$_1$ =   Temperature before helium expansion

P$_2$ =   Pressure of helium after helium expansion

V$_2$ =   Total system volume = V$_1$ + V$_{sample\ holder}$

T$_2$ =   Temperature after helium expansion

2. Determination of the methane and carbon dioxide adsorption on adsorbents

Determination of the methane and carbon dioxide adsorption was carried out at different constant temperatures; room temperature (35 °C) and pressure up to 100 psia for CH$_4$ and CO$_2$. Temperature was adjusted to room temperature (35 °C). At desired pressure, methane or carbon dioxide was introduced from a high pressure cylinder into a sample holder. During the experiment, the time to reach the equilibrium of methane and carbon dioxide adsorption was within approximately 20 and 30 min, respectively. The methane and carbon dioxide pressures were recorded before and after each methane expansion.

The ideal gas law and conservation of mass were also used for determining the amount of methane and carbon dioxide adsorbed on the adsorbents. The amounts of methane and carbon dioxide adsorbed by activated carbons can be obtained by the following equation.

$$n_{ad} = n_{ad-1} + \frac{P_1 V_1}{zRT_i} - \frac{P_{f-1} V_2}{zRT_{f-1}} - \frac{P_f(V_1 + V_2)}{zRT_f} \qquad (3.3)$$

Where   n$_{ad}$ =   Total amount methane and carbon dioxide adsorbed by activated carbons (mole)

n$_{ad-1}$ =   Amount methane and carbon dioxide adsorbed at previous stage (mole)

P$_i$ =   Initial pressure of methane and carbon dioxide before methane and carbon dioxide expansion into the sample holder (psia)

P_{f-1}	=	Final pressure of methane and carbon dioxide after methane and carbon dioxide expansion into the sample holder in the previous stage (psia)
P_f	=	Final pressure of methane and carbon dioxide after methane and carbon dioxide expansion into the sample holder (psia)
V_1	=	Volume of manifold excluding volume of sample holder (cm^3)
V_2	=	Volume of the sample holder (cm^3)
Z	=	Compressibility factor of methane and carbon dioxide
T_i	=	Initial temperature of methane and carbon dioxide before methane and carbon dioxide expansion into the sample holder (K)
T_f	=	Final temperature of methane and carbon dioxide before methane and carbon dioxide expansion into the sample holder (K)
T_{f-1}	=	Final temperature of methane and carbon dioxide before methane and carbon dioxide expansion into the sample holder in the previous stage (K)
R	=	Gas constant, 82.0578 atm·cm^3/mol·K

CHAPTER IV
RESULTS AND DISCUSSION

4.1 Adsorbent Characterization

Adsorbents used in this study were activated carbon (AC), ZIF-8, UiO-66, and MIL-53 (Al). In addition, different ratios of polyvinylidene fluoride (PVDF) with activated carbon and ZIF-8 were also investigated. PVDF is of interest in this application because it can resist to solvent, acids, and bases. Moreover, binding PVDF with adsorbents facilitates in practical applications for easy controlling and recycling. These adsorbents were characterized by Autosorb-1MP (Quantachrome Instrument), Fourier transform infrared spectroscopy (FTIR), scanning electron microscopy (SEM), and x-ray diffraction analysis (XRD).

4.1.1 N_2 Adsorption-Desorption Isotherms

Autosorb-1MP (Quantachrome Instrument) was used to measure nitrogen adsorption-desorption isotherms of adsorbents at -196 °C. The degassing of the adsorbents was previously performed at 100 °C for 12 h. The specific surface area was calculated by the Brunauer, Emmet, and Teller (BET) method, and the micropore volume was acquired by Dubinin-Radushkevich (DR) method. The total pore volume was estimated from the adsorption of nitrogen at the relative pressure of 0.99.

The N_2 adsorption and desorption isotherms of activated carbon, ZIF-8, MIL-53 (Al), and UiO-66 are shown in Figure 4.1. All isotherms at low relative pressure correspond to Type I isotherm conforming to the classification of the IUPAC classification (Donohue *et al.*, 1998). This result indicates the microporous characteristics of these adsorbents. However, the isotherm of activated carbon at a relative pressure lower than 0.2 shows a broad knee suggesting the presence of super-micropore in this sample (Blanco *et al.*, 2016). Moreover, MIL-53 (Al) and UiO-66 show Type IV isotherm according to the hysteresis loop with increasing adsorption at high relative pressure. This type of isotherm is obtained from the

presence of mesoporous structure in the adsorbent. The hysteresis loop is related with the capillary condensation of the large pore attributing to the completed filling in mesopores (Meng and Park, 2012).
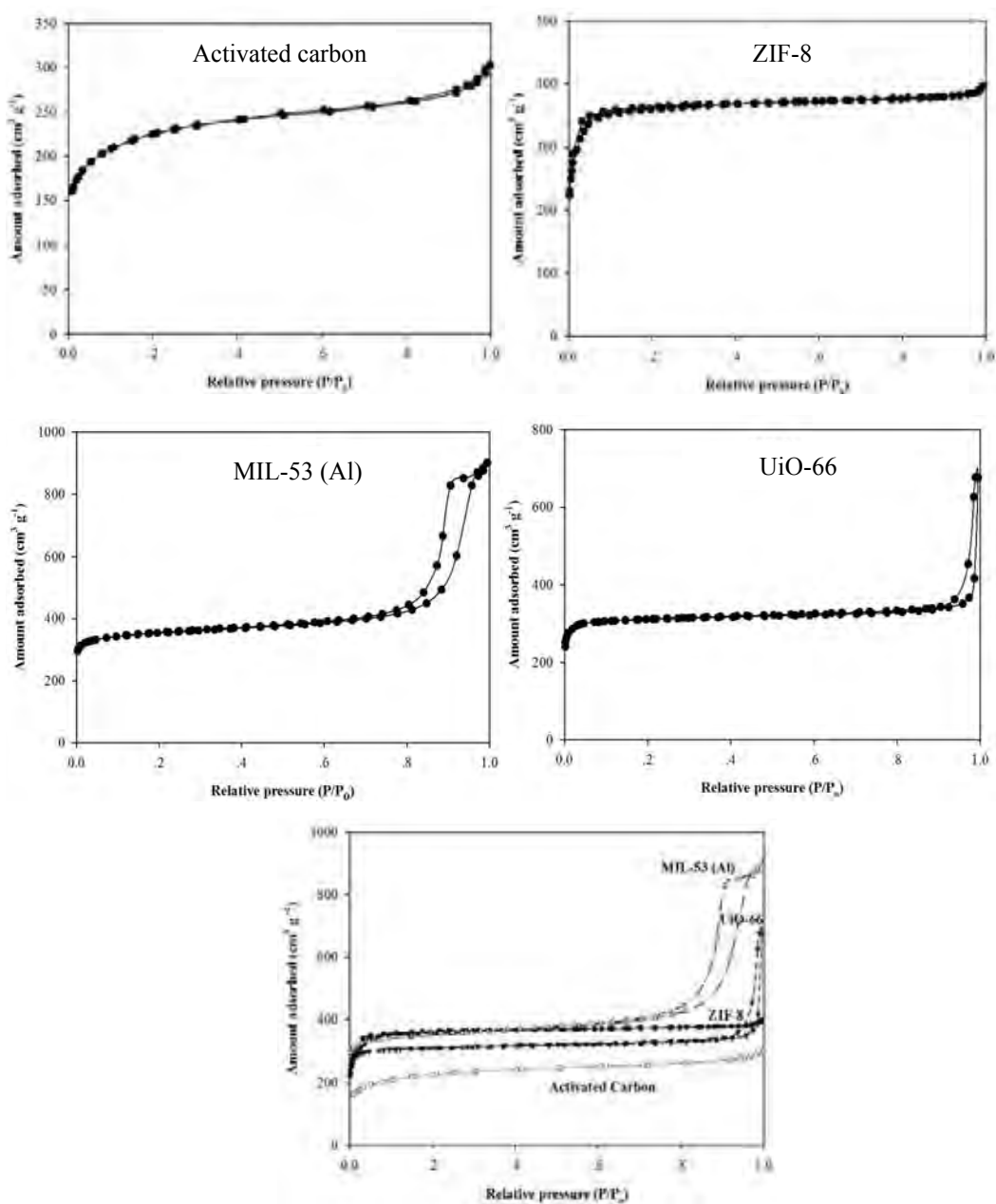
Figure 4.1 N_2 adsorption-desorption isotherms of adsorbents at -196 °C.

As shown in Figure 4.2, the addition of PVDF in ZIF-8 and activated carbon also correspond to Type I isotherm, IUPAC classification, likewise pure adsorbents. Note that the percentage in front of ZIF-8 indicates the amount of PVDF added into the sample. Figure 4.2a illustrates that ZIF-8 has higher nitrogen adsorption capacity than 75 wt% ZIF-8, 50 wt% ZIF-8, and 25 wt% ZIF-8. In the same way, nitrogen adsorption capacity of activated carbon is higher than 50 wt% AC and 25 wt% AC. It can be concluded that PVDF binder reduces the adsorption performance in these adsorbents.
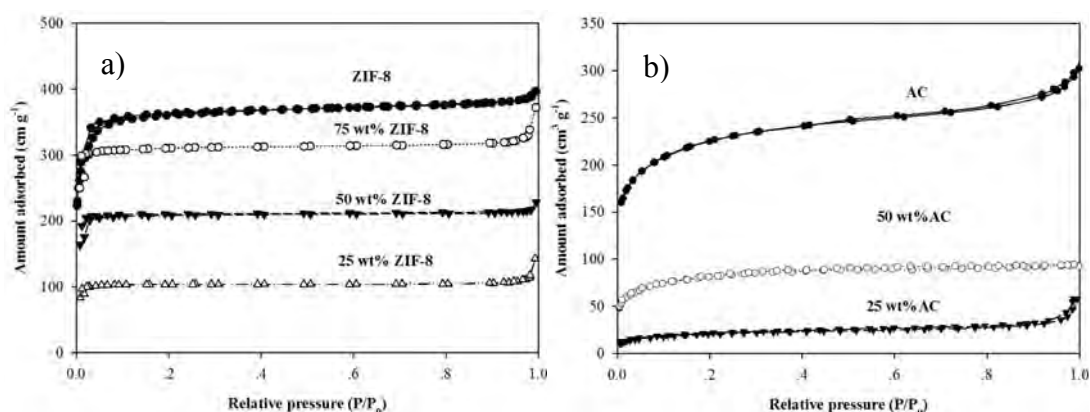
Figure 4.2 N_2 adsorption-desorption isotherms of (a) ZIF-8, 75 wt% ZIF-8, 50 wt% ZIF-8, and 25 wt% ZIF-8 and (b) activated carbon, 50 wt% activated carbon, and 25 wt% activated carbon at 30 °C ($\pm$ 2).

Table 4.1 lists the physical properties consisting of surface area (S_{bet}), micropore volume (V_{micro}) calculated by Dubinin-Radushkevich (DR) method, total pore volume (V_{Total}), average pore diameter (D_{avg}), and the ratio of micropore volume to total pore volume. It can be observed that the larger surface area corresponds to the higher micropore volume and total pore volume. Moreover, the high surface area sample shows the narrow average pore diameter. MIL-53 (Al) has the highest surface area following by UiO-66, ZIF-8, and activated carbon. MIL-53 (Al) also has the highest micropore volume. Although UiO-66 has approximately the same surface area as ZIF-8, ZIF-8 has more micropore fraction and narrower pore

size diameter than UiO-66. PVDF has almost no surface area and micropore volume resulting in no adsorption in its pores. The addition of PVDF in ZIF-8 and activated carbon results in the decrease in the surface area and micropore volume, and the decrease is proportional to the amount of PVDF added. The result also shows the decrease in the average pore diameter when the amount of PVDF decreases. Even though 75 wt% ZIF-8 has higher surface area and micropore volume than 50 wt% ZIF-8, the average pore diameter of 50 wt% ZIF-8 is lower than 75 wt% ZIF-8.

Table 4.1 Physical properties of adsorbents

Adsorbent	S_{BET} (m^2/g)	V_{Total} (cm^3/g)	V_{Micro}, DR (cm^3/g)	D_{Avg} (nm)	V_{Micro}/V_{Total}
UiO-66	1,195	1.66	0.60	6.32	0.36
MIL-53 (Al)	1,343	1.62	0.91	5.11	0.56
Activated carbon	719	0.51	0.41	2.85	0.80
50 wt% AC	300	0.24	0.17	3.30	0.71
25 wt% AC	94	0.12	0.06	4.92	0.5
ZIF-8	1,182	0.63	0.58	2.14	0.92
75 wt%ZIF-8	923	0.58	0.50	2.42	0.86
50 wt%ZIF-8	621	0.35	0.33	2.31	0.94
25 wt%ZIF-8	307	0.22	0.17	3.00	0.77
PVDF	5	0.09	0.01	76.28	0.11

In accordance with adsorbed natural gas requirements, adsorbents are the significant factor, which should have suitable characteristics. The high surface

area, high micropore volume with no void or macropore volume, narrow average pore diameter are needed. The pore size should be greater than at least 0.76 nm (two times of methane molecules). The appropriate pore size of adsorbent can support more attraction force of gas molecule and adsorbent, van der Waals forces, resulting in high methane storage capacity (Bagheri and Abedi, 2011). Therefore, ZIF-8, 75 wt% ZIF-8, UiO-66, MIL-53 (Al) and activated carbon should have selective adsorption property owing to the high surface area and high micropore volume.

4.1.2 Fourier Transform Infrared Spectroscopy

Besides the appropriate surface area, micropore volume, and pore size diameter, hydrophobicity of the surface is also significant. As reported by Hao *et al.* (2013), the adsorbents with a lower hydrophobic property have lower methane adsorption capacity. Actually, the surface area of adsorbents contains both hydrophobic and hydrophilic sites but the adsorption potential of methane prefers to hydrophobic sites owing to the non-polar nature of methane. However, carbon dioxide, a polar adsorbate, is the competition adsorbate in this experiment. The high hydrophilic sites on the adsorbent surface tend to increase the carbon dioxide adsorption capacity. Results for the Fourier transform infrared spectroscopy will show the functional group of adsorbents effecting the methane and carbon dioxide adsorption.

The characteristics of activated carbon using FTIR sprectrum are shown in Figure 4.3. The very low signal at 3500 cm^{-1} indicates the presence of O–H bond stretching. The peak at 2924 cm^{-1} shows C–H bond of the aromatic ring. Another band at 1678 cm^{-1} is the C=C bonds of an alkene compound. The CH_3 bending vibrations are observed at wavenumber of 1386 cm^{-1} (Maulidiyah *et al.*, 2015).

Figure 4.4 shows FTIR analysis indicating the characteristic absorbance of ZIF-8, constructed from 2-methylimidazole and zinc ions. The small peaks at 3135 cm^{-1} and 2934 cm^{-1} attributed to C–H stretching vibrational modes of the imidazole ring and the methyl group, which presents in the linker, respectively. The peak at 1583 cm^{-1} could be due to the C=N stretch modes. The bands in the spectral region of 500-1350 cm^{-1} are associated with aromatic sp^2 C–H bending of the

imidazole ring whereas the spectra bands in the range 1350-1500 cm^{-1} are the stretching of the imidazole ring. Basically, a strong band at 421 cm^{-1} is observed as the Zn–N stretching, which is the zinc atoms connect to nitrogen atoms during the formation of ZIF-8. However, the peak was not found due to the limited range of instrument (Kaur *et al.*, 2017).
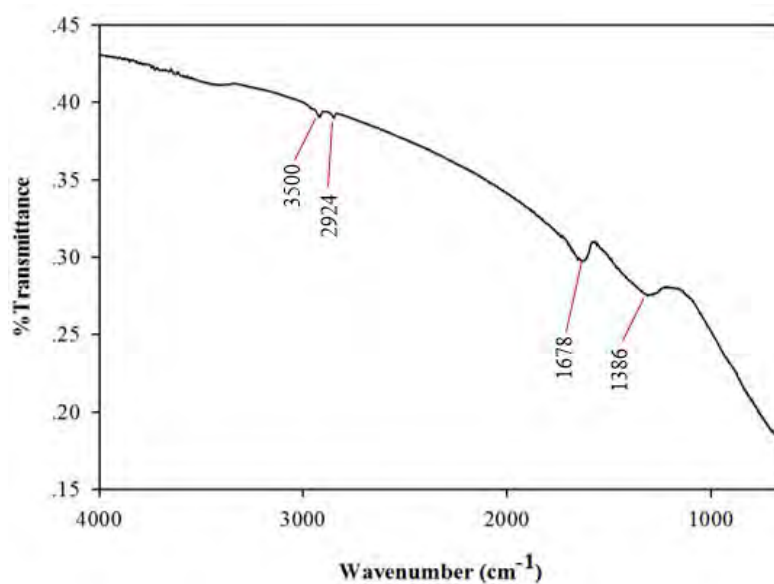

Figure 4.3 Fourier transform infrared spectroscopy of activated carbon.
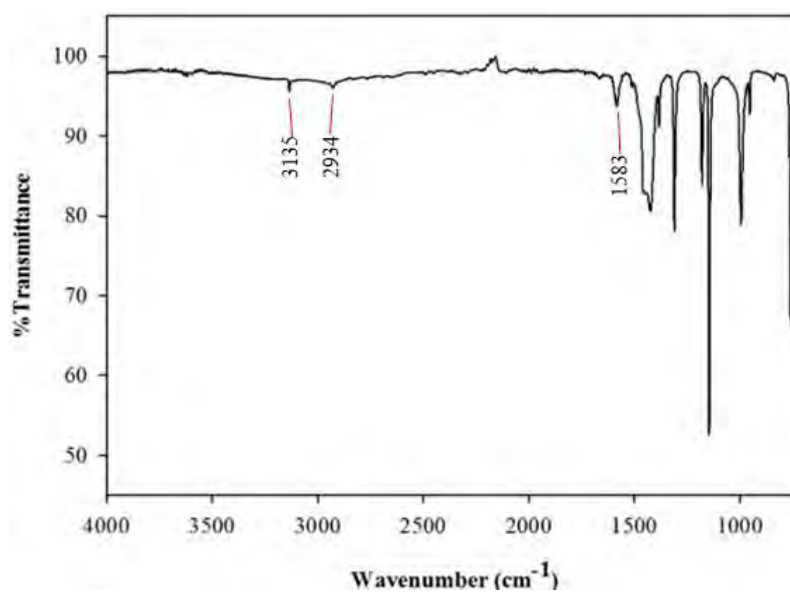
Figure 4.4 Fourier transform infrared spectroscopy of ZIF-8.
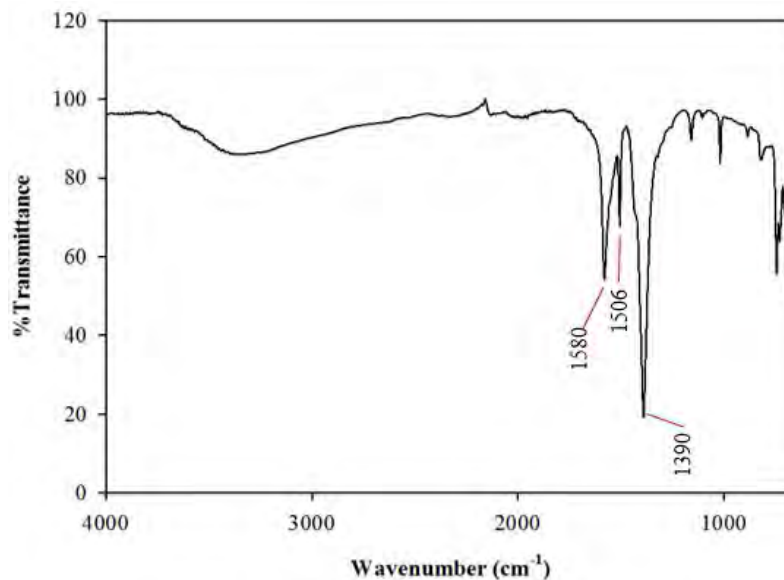
Figure 4.5 Fourier transform infrared spectroscopy of UiO-66.

The FTIR spectra of UiO-66 (zirconium-terephthalate-based MOF) are shown in Figure 4.5. This result mainly reflect the benzene-carboxylates due to its composition in UiO-66. The peak at 1580 cm^{-1} is from the C–O bonding in the carboxylate. The C=C vibration of a benzene ring is confirmed by a small band at 1506 cm^{-1}. The strong band at 1390 cm^{-1} is associated with the O–C–O symmetric stretching in the carboxylate group. The peak at 690-900 cm^{-1} is due to C–H vibration of a benzene ring (Cao *et al.*, 2015).

MIL-53 (Al) is a metal organic framework using aluminum nitrate as the aluminium source and 1,4-benzenedicarboxylic acid (H_2BDC) as the organic ligand. The characteristics of MIL-53 (Al) are shown in Figure 4.6. The band at 1610 cm^{-1} and 1510 cm^{-1} could be attributed to (C–O) asymmetric stretching. The band at 1410 cm^{-1} is symmetric carboxylate (C–O) stretching vibrations of benzene ring, which is consistent with the presence of (C–O) coordinated to aluminum. The characteristic spectra of MIL-53 (Al) are similar to the characteristic spectra of UiO-66 spectrum due to the same organic ligand (Yan *et al.*, 2015).
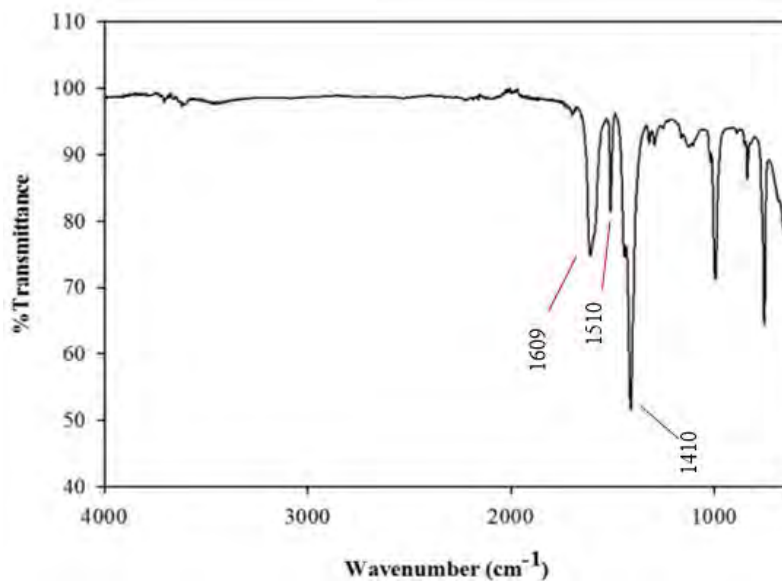
Figure 4.6 Fourier transform infrared spectroscopy of MIL-53.
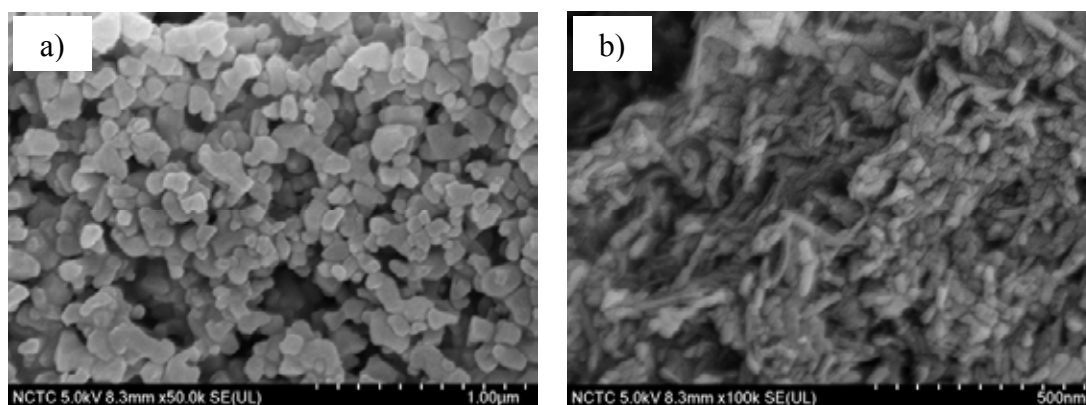
Figure 4.7 Scanning electron micrographs of (a) UiO-66 and (b) MIL-53 (Al).

4.1.3 Scanning Electron Microscopy

The topology of UiO-66 is shown in Figure 4.7a. The shape of UiO-66 resembles the morphology previously reported by Schelling *et al*. (2018). The morphology of MIL-53 (Al) is a rod-like structure, as shown in Figure 4.7b. This figure corresponds to the report by Chen *et al*. (2018).
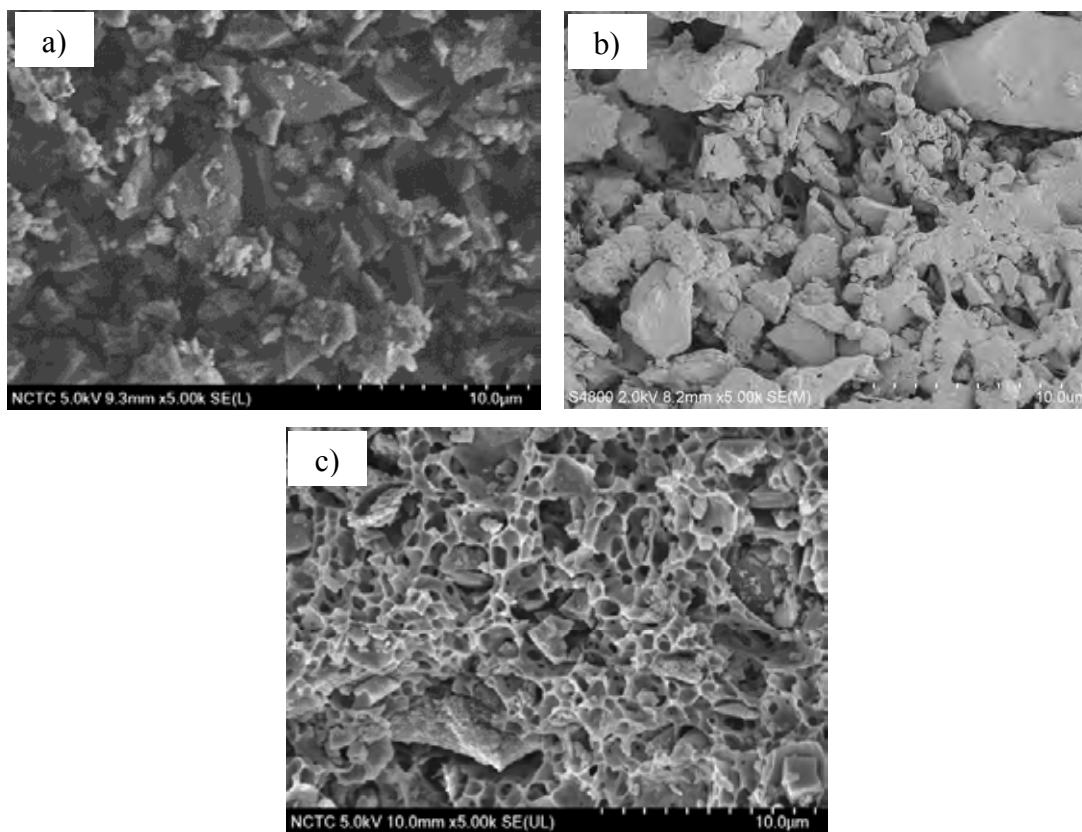
Figure 4.8 Scanning electron micrographs of (a) activated carbon (b) 50 wt% AC, and (c) 25 wt% AC.

Scanning electron microscopy (SEM) was used to investigate the morphology of activated carbon, 50 wt% AC, and 25 wt% AC. The applied voltage at 5 kV and magnification of 500 were used, and the results are shown in Figure 4.8 It confirms the amorphous structure of activated carbon, Figure 4.8a, while Figure 4.8b and 4.8c show that the addition of PVDF results in the extremely large pore size with mostly circular shape. It can be described that PVDF blocks the porosity of activated carbon. The higher percentage of PVDF indicates the higher blocked porosity of activated carbon associate with the reducing of surface area and micropore volume, as shown in Table 4.1.

The topology of ZIF-8 are illustrated in Figure 4.9a. ZIF-8 has a uniform crystalline structure. It shows the rhombic dodecahedral shape of ZIF-8. Moreover, Figure 4.9 indicates the same trend as activated carbon, which is the porosity reduction when the proportion of PVDF increases. This blockage decreases the possibility of contact between gas molecule and adsorbent wall (Mat *et al.*, 2006).
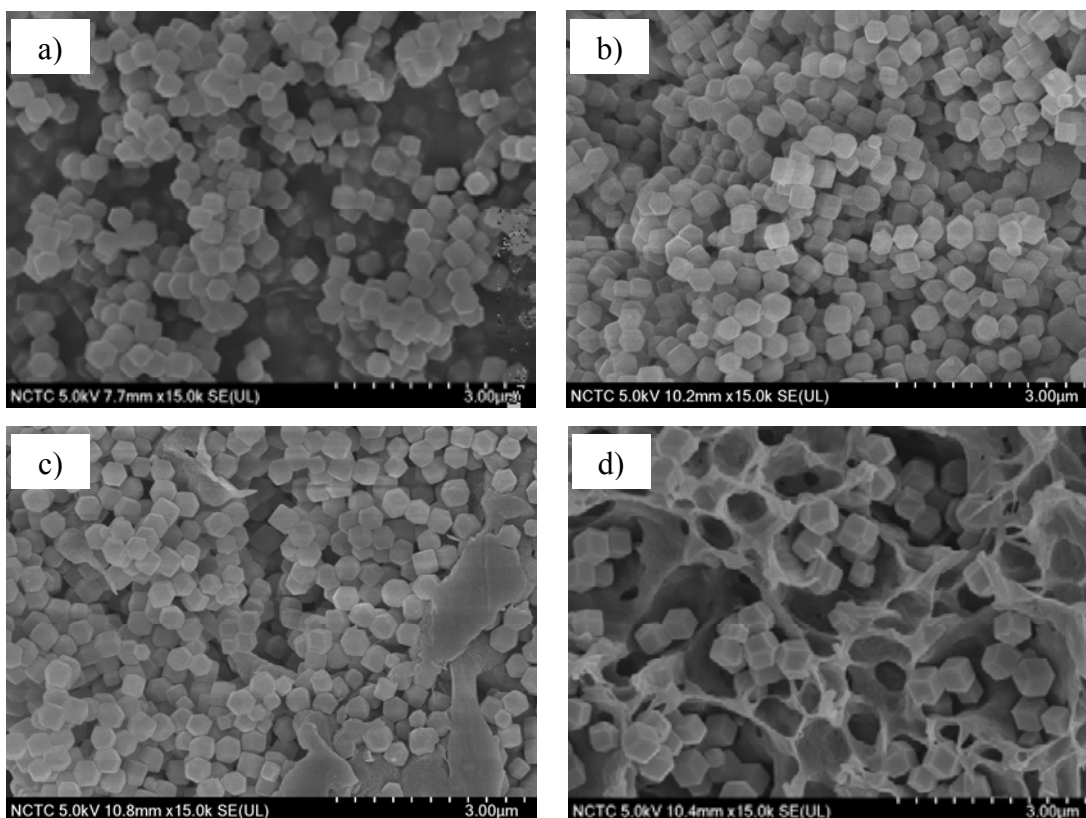
Figure 4.9 Scanning electron micrographs of ZIF-8 (a), 75 wt% ZIF-8 (b), 50 wt% ZIF-8 (c), and 25 wt% ZIF-8 (d).

4.1.4 X-ray Diffraction Analysis

Figure 4.10 illustrates the XRD pattern of ZIF-8. The formation of ZIF-8 is crystalline ZIF-8 phase corresponding with previous report, which confirmed the sodalite structure of ZIF-8 (Wee *et al*., 2014). The characteristic peak at $2\theta = 7.3°$ associats with the (011) peak of ZIF-8. This pattern indicates the highly crystalline ZIF-8 with no additional peaks detected.

The x-ray diffraction pattern of MIL-53 (Al) is illustrated in Figure 4.11. The characteristic peaks of MIL-53 (Al) are consistent with the reported XRD patterns. This result suggests the crystalline structure of MIL-53 (Al). The peak with high intensity at $2\theta = 8.7°$ and two weaker peaks with low intensity at $2\theta = 15.0°$ and $17.5°$ are corresponding to the large pore framework of the MIL-53 structure (Tien-Binh *et al*., 2015). Figure 4.12 shows the identical XRD pattern of UiO-66 confirming the existing report (Massoudinejad *et al*., 2016). The characteristic peaks of UiO-66 are $2\theta = 7°$ and $8.45°$.
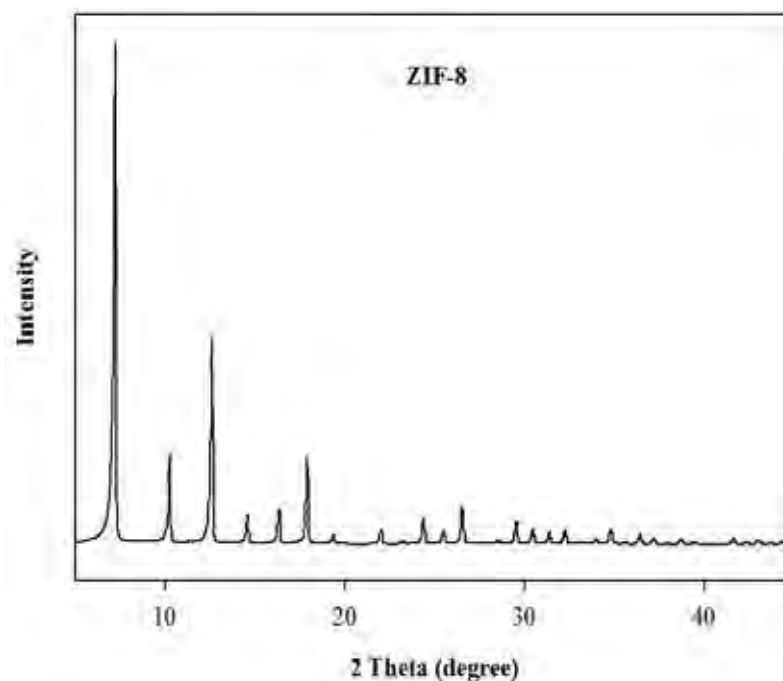
Figure 4.10 X-ray diffraction (XRD) pattern of ZIF-8.

57
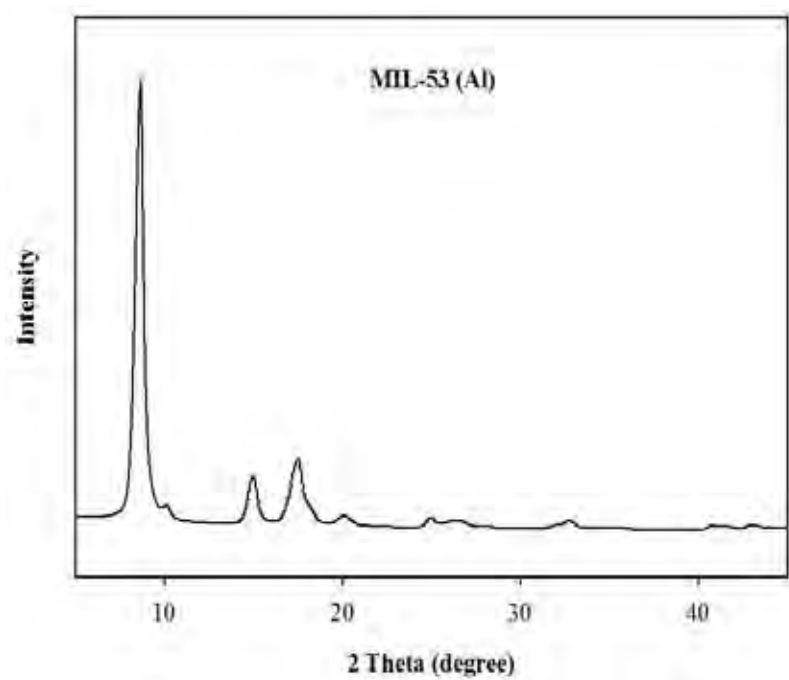
Figure 4.11 X-ray diffraction (XRD) pattern of MIL-53 (Al).
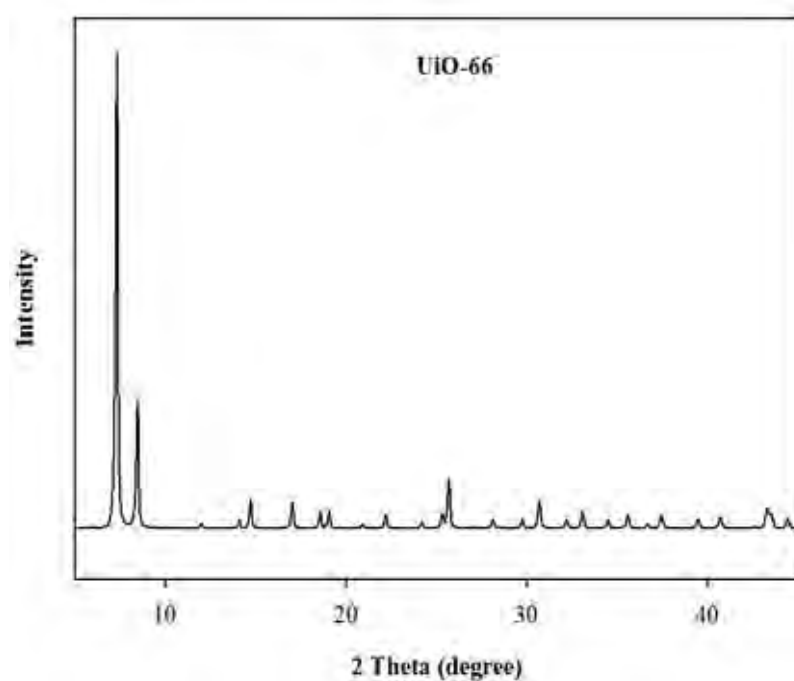
Figure 4.12 X-ray diffraction (XRD) pattern of UiO-66.

4.2 Equilibrium Adsorption of Methane on the Adsorbents

Adsorption of all adsorbents was studied at 30 °C (± 2) and variable pressure up to 100 psi with a static system. The amount of each adsorbent was fixed at 2 ml. Helium was used as a purge gas in this study. The adsorption processes were carried out using high purity methane gas. The data were recorded every after 30 minutes from 0-100 psi. Each experiment was repeated at least twice to ensure its reproducibility. Note that PVDF shows no methane adsorption.
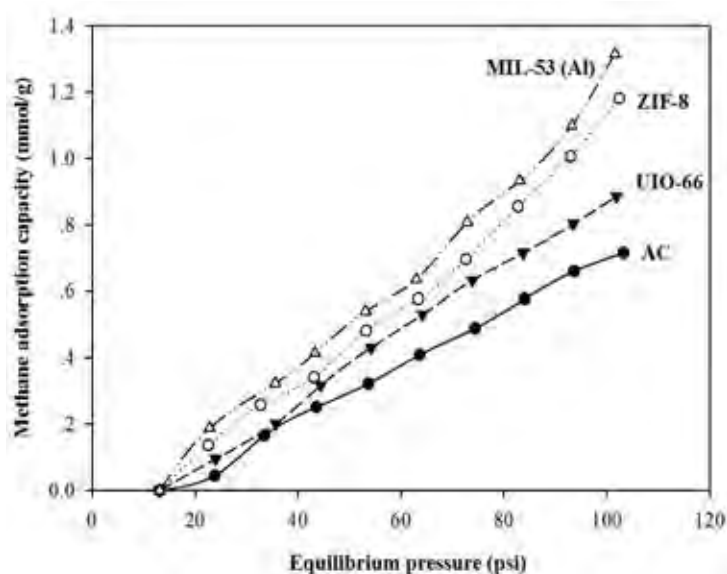
Figure 4.13 Methane adsorption on activated carbon (AC) (●), ZIF-8 (○), UiO-66 (▼), and MIL-53 (Al) (Δ) at 30 °C (± 2).

The methane adsorption capacity of pure adsorbents is shown in Figure 4.13. This graph presents the increase in the methane adsorption with the increase in the pressure because the higher pressure induces more van der Waals attraction forces between the methane molecule and the adsorbent surface as Bagheri and abedi (2011) report. MIL-53 (Al) shows the highest methane uptake followed by ZIF-8, UiO-66, and activated carbon. This result is consistent with their surface areas and micropore volumes (Figures 4.16 and 4.17). MIL-53 (Al) has the highest surface area corresponding to the highest methane adsorption. ZIF-8 adsorbs methane higher than

UiO-66 even though both adsorbents have approximately the same surface area (Figure 4.16) and micropore volume (Figure 4.17). This can be described by their micropore volume to total pore volume ratios, as shown in Table 4.1. ZIF-8 has relatively higher micropore volume to total pore volume ratios (0.92) than UiO-66 (0.36). In other words, ZIF-8 has relatively low mesopore volume. The result is in agreement with the report by Bagheri and Abedi (2011) who reported that methane is more favourable to fill in micropores than in macropores and mesopores. For further clarification, Mosher *et al*. (2013) described that the opposing wall, which the distance between pores is close enough, will have the high force field and contributes to the higher adsorption. The mesopore volume of UiO-66 is compatible with large pore size diameter of UiO-66 (Table 4.1). The result shows that not only the surface area and micropore volume affect the methane adsorption but also the ratio of micropore volume to total pore volume. Additionally, the activated carbon has the lowest methane storage owing to its lowest surface area and micropore volume (Figures 4.16 and 4.17).

Methane adsorption capacities of activated carbon, 25 wt% AC, and 50 wt% AC are shown in Figure 4.14. The activated carbon has higher methane adsorption capacity than 50 wt% AC and 25 wt% AC, respectively. The methane uptake decreases with the amount of the activated carbon, and that corresponds to the surface area and micropore volume explained by Figures 4.16 and 4.17, owing to the blockage of adding PVDF. This blockage can be observed in Figure 4.8.

Figure 4.15 illustrates methane adsorption capacities of ZIF-8, 75 wt% ZIF-8, 50 wt% ZIF-8, and 25 wt% ZIF-8. ZIF-8 has the highest methane adsorption capacity followed by 75 wt% ZIF-8, 50 wt% ZIF-8, and 25 wt% ZIF-8. The lower methane adsorption is consistent with the decrease in the amount of ZIF-8 in the sample. As shown in Figures 4.16 and 4.17, the surface area and micropore volume decrease with the decrease in the ZIF-8 content. The blockage of PVDF inside porous ZIF-8 may cause the decreased in the surface area corresponding to the morphology, as shown in Figure 4.9.

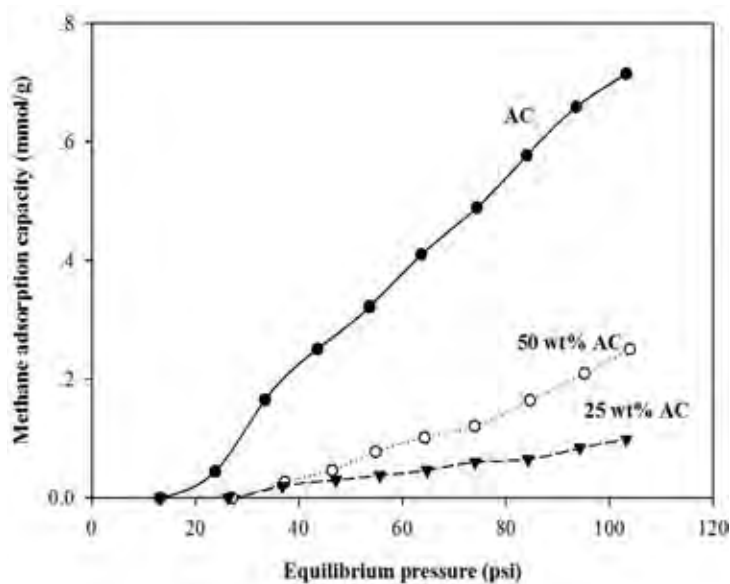**Figure 4.14** Methane adsorption on activated carbon (AC) (●), 50 wt% AC (○), and 25 wt% AC (▼) at 30 °C (± 2) (the percentage in front of activated carbon indicates the amount of activated carbon mixed with PVDF).
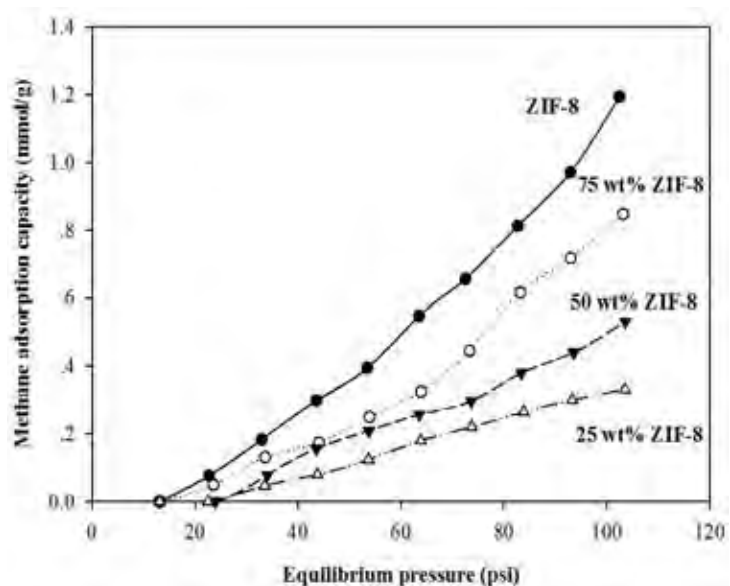
Figure 4.15 Methane adsorption on ZIF-8 (●), 75 wt% ZIF-8 (○), 50 wt% ZIF-8 (▼), and 25 wt% ZIF-8 (Δ) at 30 °C (± 2) (the percentage in front of ZIF-8 indicates the amount of ZIF-8 mixed with PVDF).

Table 4.2 Different adsorption capacity between adsorbents and adsorbents with the PVDF binder

Adsorbent	Methane Adsorption (mmol/g)	%Diff
AC	0.71	-
50 wt% AC	0.25	64.79
25 wt% AC	0.1	85.92
ZIF-8	1.18	-
50 wt% ZIF-8	0.53	55.08
25 wt% ZIF-8	0.33	72.03

The effect of adding PVDF on the activated carbon and ZIF-8 is further described in Table 4.2. This table shows the different percentage (%Diff) on methane adsorption between the adsorbents and those with the PVDF binder. %Diff of 50 wt% AC is higher than 50 wt% ZIF-8. In the same way, %Diff of 25 wt% AC is also higher than 25 %wt ZIF-8. This result indicates that the effects of PVDF are different on different adsorbents. It may be deduced that the reduction of methane adsorption by the PVDF binder on the amorphous structure (AC) is higher than the crystalline structure (ZIF-8).

Figures 4.16 and 4.17 describe that the surface area and micropore volume mainly affect to the methane adsorption. MIL-53 has the highest methane capacity (3.25 mmol/g) and 25 wt% AC has the lowest methane capacity (0.01 mmol/g). Nonetheless, some adsorbents have similar surface area and micropore volume as in the case of UiO-66 and ZIF-8, and 25 wt% ZIF-8 and 50 wt% AC, but the adsorption capacities are different. These phenomenon can be explained by the effects of micropore volume to total pore volume ratio and average pore diameter as mentioned before. The higher micropore volume to total pore volume ratio and lower average pore diameter, the higher the methane adsorption.
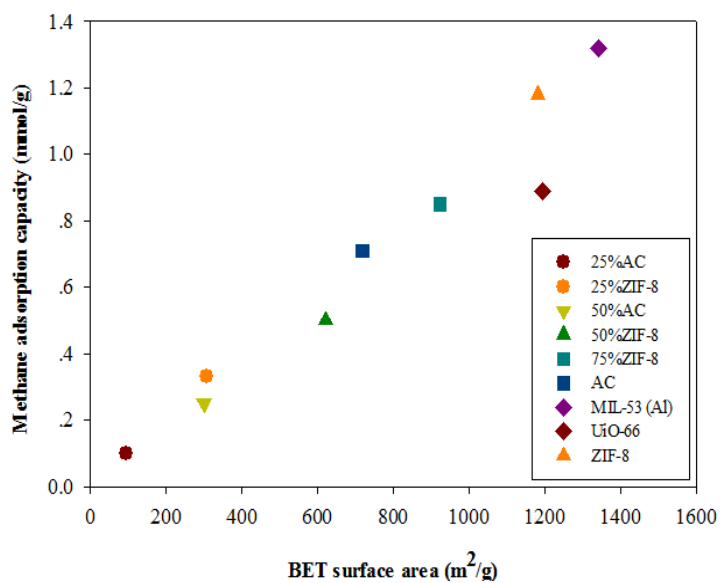
Figure 4.16 Methane adsorption capacity (mmol/g) as a function of BET surface area (m²/g) at 100 psi and 30 °C (± 2).
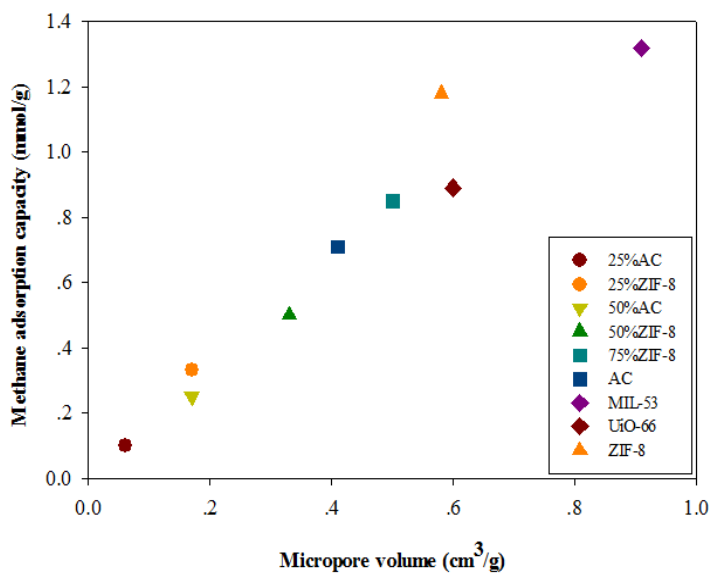
Figure 4.17 Methane adsorption capacity (mmol/g) as a function of micropore volume (cm³/g) at 100 psi and 30 °C (± 2).

4.3 Equilibrium Adsorption of Carbon Dioxide on the Adsorbents

Carbon dioxide adsorption on activated carbon, ZIF-8, UiO-66, and MIL-53 (Al) is shown in Figure 4.18. In general, the adsorption capacity increases with the pressure over the experimental condition. It can be observed that the carbon dioxide adsorption on MIL-53 (Al) is the highest followed by UiO-66, ZIF-8 and activated carbon. The effects of the surface area and the micropore volume on the adsorption can be described using Figures 4.19 and 4.20. The larger the surface area and micropore volume, the higher the carbon dioxide adsorption. Apart from the surface area and micropore volume, the open metal sites and organic ligands can facilitate interaction with polarizable carbon dioxide molecules and enhance carbon dioxide adsorption since they allow close approach of carbon dioxide to the pore surface as described by Sumida *et al.* (2012). Canepa *et al.* (2013) reported that different metal atoms show different carbon dioxide interaction to MOFs. It was observed that Al atom has much larger interaction to oxygen atom from carbon dioxide molecules than Zr atom and Zn atom. Correspondingly, MIL-53 consisting of Al atoms has the highest carbon dioxide adsorption.

Figure 4.18 Carbon dioxide adsorption on activated carbon (○), ZIF-8 (●), MIL-53 (Al) (▼), and UiO-66 (Δ) at 30 °C (± 2).

Figure 4.19 Carbon dioxide adsorption capacity (mmol/g) as a function of BET surface area (m^2/g) at 100 psi and 30 °C ($\pm$ 2).
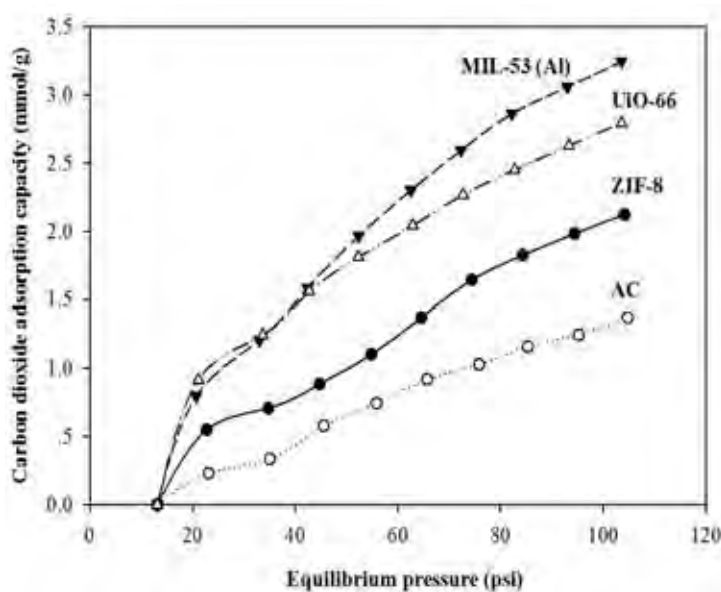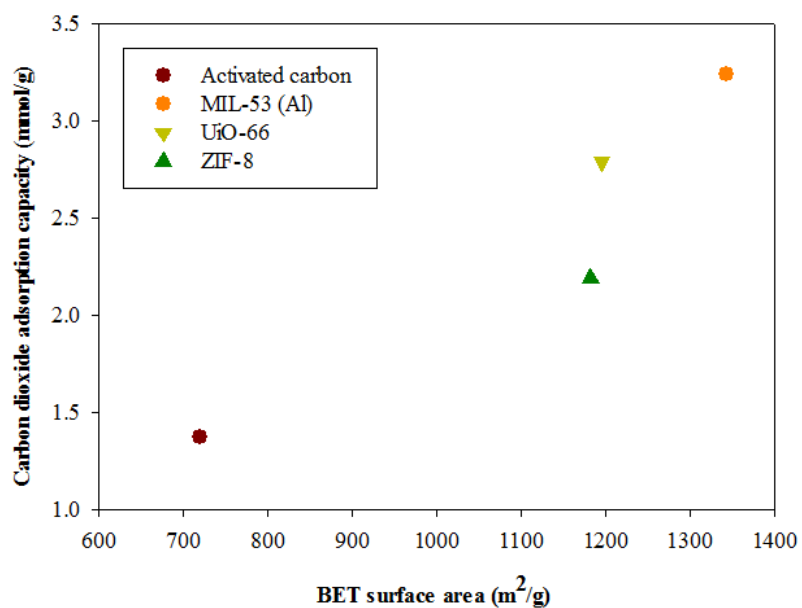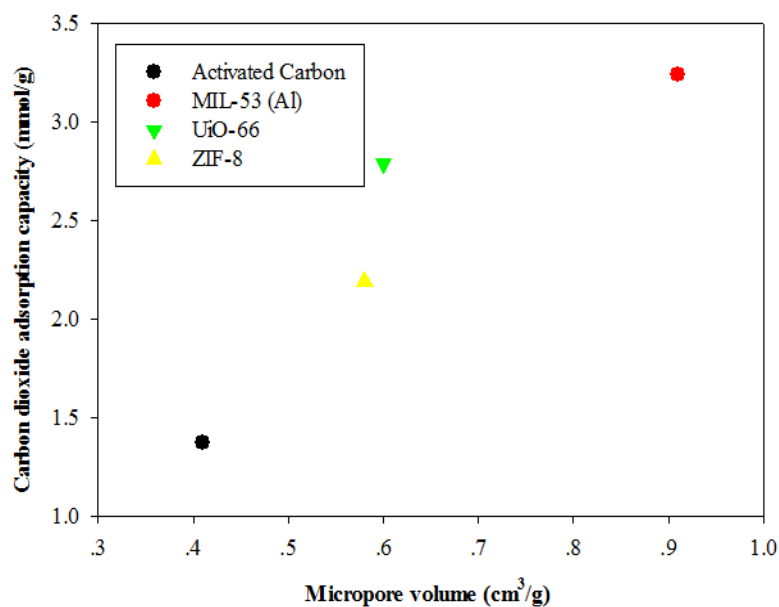

Figure 4.20 Carbon dioxide adsorption capacity (mmol/g) as a function of micropore volume (cm^3/g) at 100 psi and 30 °C ($\pm$ 2).

Unlike the methane adsorption on UiO-66 and ZIF-8, where the former shows lower adsorption capacity than the latter, the carbon dioxide adsorption on the two adsorbents shows the opposite trend. From Figures 4.19 and 4.20, the carbon dioxide adsorption on UiO-66 is higher than ZIF-8, even though the surface areas and micropores are similar. As described in the previous part, ZIF-8 adsorbs methane higher than UIO-66 owing to the effect of micropore volume to total pore volume ratio. However, the effect of micropore volume to total pore volume ratio on the carbon dioxide adsorption is quite low, or other factors may govern the mechanism. It can be seen in Figure 4.21 that ZIF-8 and UiO-66 have different bridging ligands and open metal sites. The organic ligand of ZIF-8 is methylImidazodolate with Zn atom. UiO-66 consists of Zr atom bridged by 1,4-benzene-dicarboxylate (BDC) linkers. As stated by Canepa *et al.* (2013), the carbon dioxide adsorption energy of Zn atom is close to Zr atom, which may indicate the similar interaction between the open metal site and carbon dioxide. However, the carbon dioxide interaction with the metal sites also depends on the amount of open metal sites. In addition, the different organic ligand indicates a different interaction toward carbon dioxide. The oxygen atoms from carbon dioxide molecule can form close contacts with both the methyl groups and the imidazolates of ZIF-8 (Fisher and Bell, 2014). In addition, Liu *et al.* (2012) explained that the oxygen atom (CO_2) mainly interacts to delocalized aromatic π system of UiO-66. The different interactions determine the magnitude of force inducing the carbon dioxide adsorption.

The lowest carbon dioxide adsorption of activated carbon is consistent with its low surface area and micropore volume. Activated carbon highly composes of carbon atom with no functionality in contrast to the metal organic frameworks consisting of metal ion and organic ligand. Therefore, the characteristic of activated carbon may lower its adsorption towards carbon dioxide than metal organic frameworks.

Figures 4.19 and 4.20 indicate that the surface area and micropore volume mainly influence the carbon dioxide adsorption as same as the methane adsorption. MIL-53 (Al) has highest carbon dioxide adsorption, and the activated carbon shows lowest carbon dioxide adsorption. However, the difference structure of adsorbents

plays a more important role on the carbon dioxide adsorption than the micropore volume to total pore volume ratio as in the case of UiO-66 and ZIF-8. Therefore, the appropriate open metal site and organic ligand should result in higher carbon dioxide adsorption.
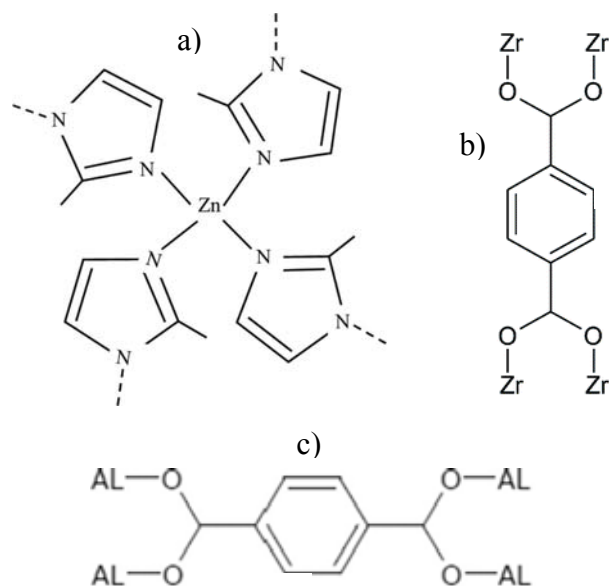
Figure 4.21 Structure of (a) ZIF-8, (b) UiO-66, and (c) MIL-53 (Al).

4.4 Comparative Adsorption of Methane and Carbon Dioxide on the Adsorbents

Though methane and carbon dioxide adsorption on the adsorbents are only physical adsorption, it is noticeable from Figure 4.22 that the carbon dioxide uptake in this study is 2 - 2.5 times greater than the methane uptake. The carbon dioxide is selectively adsorbed on the adsorbents owing to its properties. Firstly, carbon dioxide has higher critical temperature (T_c) than methane ($T_{c, CO2}$ = 31.21 °C, $T_{c, CH4}$ = -82 °C). Then, carbon dioxide behaves like a condensate steam or less volatile resulting in more opportunity to be adsorbed on the adsorbents. Furthermore, polarizability of carbon dioxide enhances the gas molecule and pore wall attractive force since electron cloud of carbon dioxide can move or relocate easily. Meanwhile, the weaker octopole of methane is expected to play a far less important part in

relation to dispersion forces (Nicholson and Gubbins, 1996). For instance, most adsorbents, such as activated carbon and MIL-53 (Al), compose of benzene rings. The interactions between the benzene rings and quadrupole of carbon dioxide are dominated by the π–π interactions (Chen *et al.*, 2013). Hence, the adsorbents can interact with carbon dioxide via van der Waals forces and also the π effect. In contrast, methane with no quadrupole moment interacts to the adsorbent only by van der Waal forces. In addition, the open metal sites in the adsorbents enhance the carbon dioxide adsorption compared with the methane adsorption. These reasons contribute to the higher carbon dioxide adsorption on the adsorbents.
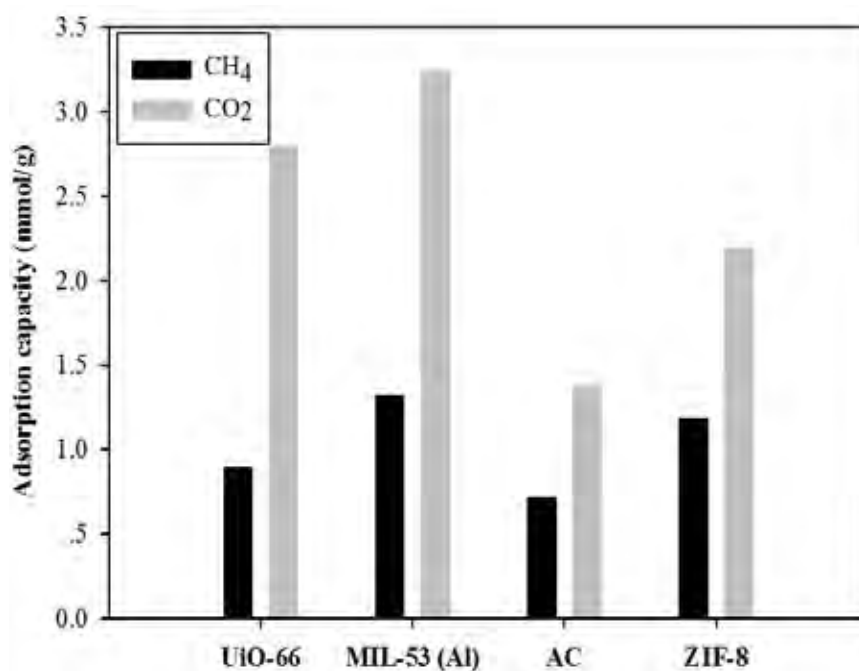
Figure 4.22 Adsorption of methane and carbon dioxide on UiO-66, MIL-53 (Al), activated carbon (AC), and ZIF-8 at 100 psi and 30 °C ($\pm$ 2).

Table 4.3 Summary of methane and carbon dioxide adsorption at 100 psi and 30 °C ($\pm$ 2)

Adsorbent	CH$_4$ Adsorption (mmol/g)	CO$_2$ Adsorption (mmol/g)	CH$_4$/CO$_2$ Selectivity
UiO-66	0.89	2.79	0.32
MIL-53 (Al)	1.32	3.24	0.41
Activated carbon	0.71	1.37	0.52
ZIF-8	1.18	2.19	0.54

The CH$_4$/CO$_2$ selectivity is shown in Table 4.3. Activated carbon and ZIF-8 have about the same selectivity, which is higher than that of MIL-53 (Al) and UiO-66. MIL-53 (Al) has lower CH$_4$/CO$_2$ selectivity resulted from the open metal sites and organic ligand, which is favourable for carbon dioxide adsorption. In addition, UiO-66 has the lowest CH$_4$/CO$_2$ selectivity owing to its large pore size diameter. In other words, the gas-gas interaction in large pores is weaker than in small pores obstructing the methane adsorption. However the carbon dioxide adsorption on UiO-66 is still high because the metal site and organic ligand play a more important role than the pore size diameter.

CHAPTER V
CONCLUSIONS AND RECOMMENDATIONS

5.1 Conclusions

Comparative adsorption of methane and carbon dioxide on activated carbon ZIF-8, UiO-66, and MIL-53 (Al) at 35 °C and up to 100 psi was studied. The effects of PVDF binder with ZIF-8 and activated carbon were also investigated including 75 wt% ZIF-8, 50 wt% ZIF-8, 25 wt% ZIF-8, 50 wt% ZIF-8, and 25 wt% ZIF-8. MIL-53 (Al) has the highest methane adsorption followed by ZIF-8, UiO-66, and activated carbon. Not only are surface area and micropore volume important for methane adsorption, but also the high micropore volume to total pore volume ratio. UiO-66 and ZIF-8 have about the same surface area and micropore volume but ZIF-8 shows higher methane adsorption due to its higher micropore volume to total pore volume ratio. The addition of PVDF decreases the methane adsorption. Additionally, the PVDF binder in activated carbon affects the methane adsorption at a higher extent than that in ZIF-8. The carbon dioxide adsorption is also governed by the surface area and micropore volume. MIL-53 (Al) has higher carbon dioxide adsorption than UiO-66, ZIF-8, and activated carbon. The chemical properties, such as open metal site and organic ligand, also influence for more carbon dioxide adsorption. All adsorbents adsorb higher carbon dioxide than methane. The CH_4/CO_2 selectivity of ZIF-8 is the highest and approximately the same as activated carbon. In summary, the appropriate adsorbent with high surface area, high micropore volume and low mesopores volume, narrow average pore size, and proper open metal site and organic linker is required for high CH_4/CO_2 selectivity.

5.2 Recommendations

5.2.1 Different binders should be studied to increase the strength of pellets with little effects on methane adsorption.

5.2.2 Because the CH_4/CO_2 selectivity in this study is low, various metal organic frameworks such as the appropriate open metal sites should be investigated for further study.

REFERENCES

Arami-Niya, A., Daud, W.M.A.W., and Mjalli, F.S. (2011) Comparative study of the textural characteristics of oil palm shell activated carbon produced by chemical and physical activation for methane adsorption. Chemical Engineering Research and Design 89(6), 657-664.

Bagheri, N. and Abedi, J. (2011) Adsorption of methane on corn cobs based activated carbon. Chemical Engineering Research and Design 89(10), 2038-2043.

Bansal, C.R. and Goyal, M. (2005) Chapter 1-activated carbon and its surface structure. Activated Carbon Adsorption, 1-65.

Beckner, M. and Dailly, A. (2016) A pilot study of activated carbon and metal-organic frameworks for methane storage. Applied Energy 162, 506-514.

Bimbo, N., Physick, A.J., Noguera-Díaz, A., Pugsley, A., Holyfield, L.T., Ting, V.P., and Mays, T.J. (2015) High volumetric and energy densities of methane stored in nanoporous materials at ambient temperatures and moderate pressures. Chemical Engineering Journal 272, 38-47.

Blanco, A.A.G., Vallone, A.F., Korili, S.A., Gil, A., and Sapag, K. (2016) A comparative study of several microporous materials to store methane by adsorption. Microporous and Mesoporous Materials 224, 323-331.

Borah, B., Zhang, H., and Snurr, R.Q. (2015) Diffusion of methane and other alkanes in metal-organic frameworks for natural gas storage. Chemical Engineering Science 124, 135-143.

Canepa, P., Arter, C.A., Conwill, E.M., Johnson, D.H., Shoemaker, B.A., Soliman, K.Z., and Thonhauser, T. (2013) High-throughput screening of small-molecule adsorption in MOF. Journal of Materials Chemistry A 1, 13597-13604

Cao, Y., Zhao, Y., Lv, Z., Song, F., and Zhong, Q. (2015) Preparation and enhanced CO_2 adsorption capacity of UiO-66/graphene oxide composites. Journal of Industrial and Engineering Chemistry 27, 102-107.

Chen, L., Cao, F., and Sun, H. (2013) Ab initio study of the p–p interactions between CO_2 and benzene, pyridine, and pyrrole. International Journal of Quantum Chemistry 113, 2261–2266.

Chen, Y., Zhang, F., Wang, Y., Tang, C., Yang, J., and Li, J. (2018) Recyclable ammonia uptake of a MIL series of metal-organic frameworks with high structural stability. Microporous and Mesoporous Materials 258, 170-177.

Curran, S.J., Wagner, R.M., Graves, R.L., Keller, M., and Green, J.B. (2014) Well to-wheel analysis of direct and indirect use of natural gas in passenger vehicles. Energy 75, 194-203.

Djeridi, W., Ben Mansour, N., Ouederni, A., Llewellyn, P.L., and El Mir, L. (2017) Study of methane and carbon dioxide adsorption capacity by synthetic nanoporous carbon based on pyrogallol-formaldehyde. International Journal of Hydrogen Energy 42(13), 8905-8913.

Djeridi, W., Ouederni, A., Wiersum, A.D., Llewellyn, P.L. and El Mir, L. (2013) High pressure methane adsorption on microporous carbon monoliths prepared by olives stones. Materials Letters 99, 184-187.

Donohue, M.D. and Aranovich, G.L. (1998) Classification of Gibbs adsorption isotherms. Advances in Colloid and Interface Science 76-77, 137-152.

Esteves, I.A.A.C., Lopes, M.S.S., Nunes, P.M.C., and Mota, J.P.B. (2008) Adsorption of natural gas and biogas components on activated carbon. Separation and Purification Technology 62(2), 281-296.

Fischer, M. and Bell, R.G. (2014) Interaction of hydrogen and carbon dioxide with sod-type zeolitic imidazolate frameworks: a periodic DFT-D study. Crystal Engineering Communications 16, 1934-1949.

Fletcher, A.J., Yüzak, Y. and Thomas, K.M. (2006) Adsorption and desorption kinetics for hydrophilic and hydrophobic vapors on activated carbon. Carbon 44(5), 989-1004.

Hao, S., Wen, J., Yu, X., and Chu, W. (2013) Effect of the surface oxygen groups on methane adsorption on coals. Applied Surface Science 264, 433-442.

Himeno, S., Komatsu, T., and Fujita, S. (2005) High-pressure adsorption equilibria of methane and carbon dioxide on several activated carbon. Chemical Engineering Journal 50, 369-376.

Jeong, Y., Fan, M., Singh, S., Chuang, C.-L., Saha, B., and Hans van Leeuwen, J. (2007) Evaluation of iron oxide and aluminum oxide as potential arsenic(V) adsorbents. Chemical Engineering and Processing: Process Intensification 46(10), 1030-1039.

Kaur, H., Mohanta, G.C., Gupta, V., Kukkar, D., and Tyagi, S. (2017) Synthesis and characterization of ZIF-8 nanoparticles for controlled release of 6-mercaptopurine drug. Journal of Drug Delivery Science and Technology 41, 106-112.

Kayal, S., Sun, B., and Chakraborty, A. (2015) Study of metal-organic framework MIL-101(Cr) for natural gas (methane) storage and compare with other MOFs (metal-organic frameworks). Energy 91, 772-781.

Khamehchi, E., Yousefi, S.H., and Sanaei, A. (2012) Selection of the best efficient method for natural gas storage at high capacities using TOPSIS method. Gas Processing Journal 1(1), 9-18.

Khan, M.I., Yasmin, T., and Shakoor, A. (2015) Technical overview of compressed natural gas (CNG) as a transportation fuel. Renewable and Sustainable Energy Reviews 51, 785-797.

Kumar, A. (2011) Adsorption of methane activated carbon by volumetric method. National Institute of Technology.

Kumar, P., Deep, A., and Kim, K.-H. (2015) Metal organic frameworks for sensing applications. TrAC Trends in Analytical Chemistry 73, 39-53.

Li, B., Wen, H.-M., Zhou, W., Xu, Jeff Q., and Chen, B. (2016) Porous Metal organic frameworks: promising materials for methane storage. Chem 1(4), 557-580.

Liu, Y., Liu, J., Chang, M., and Zheng, C. (2012) Theoretical studies of CO_2 adsorption mechanism on linkers of metal–organic frameworks. Fuel 95, 521-527.

Lozano-Castelló, D., Alcañiz-Monge, J., de la Casa-Lillo, M.A., Cazorla-Amorós, D., and Linares-Solano, A. (2002) Advances in the study of methane storage in porous carbonaceous materials. Fuel 81(14), 1777-1803.

Massoudinejad, M., Ghaderpoori, M., Shahsavani, A., and Amini, M.M. (2016) Adsorption of fluoride over a metal organic framework Uio-66

functionalized with amine groups and optimization with response surface methodology. Journal of Molecular Liquids 221, 279–286.

Mat, H.B., Zakaria, Z., and Paou, T.G. (2006) The development of adsorbent based natural gas storage for vehicle application. Project Report, Faculty of Chemical and Natural Resources Engineering, Technological University Malaysia, Kuala Lumpur, Malaysia.

Maulidiyah, Wibowo, D., Salamba, R., and Nurdin, M. (2015) Preparation and characterization of activated carbon from coconut shell - doped TiO_2 in water medium. Oriental Journal of Chemistry 31(4), 2337-2342.

Meng, L and Park, S. (2012) Investigation of narrow pore size distribution on carbon dioxide capture of nanoporous carbons. Bulletin of the Korean Chemical Society 33(11), 3749-3754.

Mosher, K., He, J., Liu, Y., Rupp, E., and Wilcox, J. (2013) Molecular simulation of methane adsorption in micro- and mesoporous carbons with applications to coal and gas shale systems. International Journal of Coal Geology 109-110, 36-44.

Nicholson, D. and Gubbins, K. E. (1996) Separation of carbon dioxide-methane mixtures by adsorption: Effects of geometry and energetics on selectivity. The Journal of chemical physics 104(20), 8126-8134.

Rada, Z.H., Abid, H.R., Shang, J., He, Y., Webley, P., Liu, S., Sun, H., and Wang, S. (2015) Effects of amino functionality on uptake of CO_2, CH_4 and selectivity of CO_2/CH_4 on titanium based MOFs. Fuel 160, 318-327.

Schelling, M., Kim, M., Otal, E., and Hinestroza, J. (2018) Decoration of cotton fibers with a water-stable metal–organic framework (UiO-66) for the decomposition and enhanced adsorption of micropollutants in water. Bioengineering 5, 14.

Shen, J., Sulkowski, J., Beckner, M., and Dailly, A. (2015) Effects of textural and surface characteristics of metal-organic frameworks on the methane adsorption for natural gas vehicular application. Microporous and Mesoporous Materials 212, 80-90.

Solar, C., Garcia, A., Vallone, A., and Sapag, K. (2010) Adsorption of methane in porous materials as the basis for the storage of natural gas. Natural Gas, 978-953-307-112-971.

Sumida, K., Rogow, D.L., Mason, J.A., McDonald, T.M., Bloch, E.D., Herm, Z.R. Bae, T., and Long, J.R. (2012) Carbon dioxide capture in metal organic frameworks. Chemical Reviews 112, 724-781.

Teo, H.W.B., Chakraborty, A., and Kayal, S. (2017) Evaluation of CH_4 and CO_2 adsorption on HKUST-1 and MIL-101(Cr) MOFs employing Monte Carlo simulation and comparison with experimental data. Applied Thermal Engineering 110, 891-900.

Tien-Binh, N., Vinh-Thang, H., Chen, X.Y., Rodrigue, D., and Kaliaguine, S. (2015) Polymer functionalization to enhance interface quality of mixed matrix membranes for high CO_2/CH_4 gas separation. Journal of Materials Chemistry A 3, 15202-15213.

Wee, L.H., Janssens, N., Sree, S.P., Wiktor, C., Gobechiya, E., Fischer, R.A., Kirschhocka, C.E.A., and Martensa, J.A. (2014) Local transformation of ZIF-8 powders and coatings into ZnO nanorods for photocatalytic application. Nanoscale 6, 2056-2060.

Yan, J., Jiang, S., Ji, S., Shi, D., and Cheng, H. (2015) Metal-organic framework MIL-53(Al): synthesis, catalytic performance for the Friedel-Crafts acylation, and reaction mechanism. Chemistry 58(10), 1544-1552.

Zakaria, Z. and George, T. (2011) The performance of commercial activated carbon adsorbent for adsorbed natural gas storage. International Journal of Recent Research and Applied Studies 9(2), 225-230.

Alberta Energy. What is natural gas?. http://www.energy.alberta.ca/NaturalGas/723. asp, last visited on 1 June 2017.

Emaze. Adsorption and desorption. www.emaze.com/@AOLFLLIT/MassTransfer1. pptx, last visited on 5 June 2016.

Enclocypedia Britannica. Adsorption. www.britannica.com/science/adsorption, last visited on 5 June 2017.

Geoplin. Natural gas and its use. www.geoplin.si/en/natural-gas/natural-gas-and-its-uses, last visited on 1 June 2017.

Howstuffworks. How natural gas vehicles work. http://auto.howstuffworks.com/fuel-efficiency/alternative-fuels/ngv3.htm, last visited on 1 June 2017.

Imperial. Natural gas 101. www.imperialoil.ca/enca/company/operations/other operations/natural-gas-1017, last visited on 15 June 2017.

Kavalov, B. (2011). Techno-economic analysis of natural gas application as an energy source for road transport in the EU. www.edis.sk/ekes/eur21last, last visited on 1 June 2017.

MEDAAD. Activated carbon application. http://medaad.com/ activated-carbon/, last visited on 7 June 2017.

U.S. Energy information administration. International Energy Outlook 2016. www.eia.gov/outlooks/ieo/, last visited on 1 June 2017.

U.S. Energy information administration. Natural gas explain. www.eia.gov/energy explained/?page=natural_gas_home, last visited on 1 June 2017.

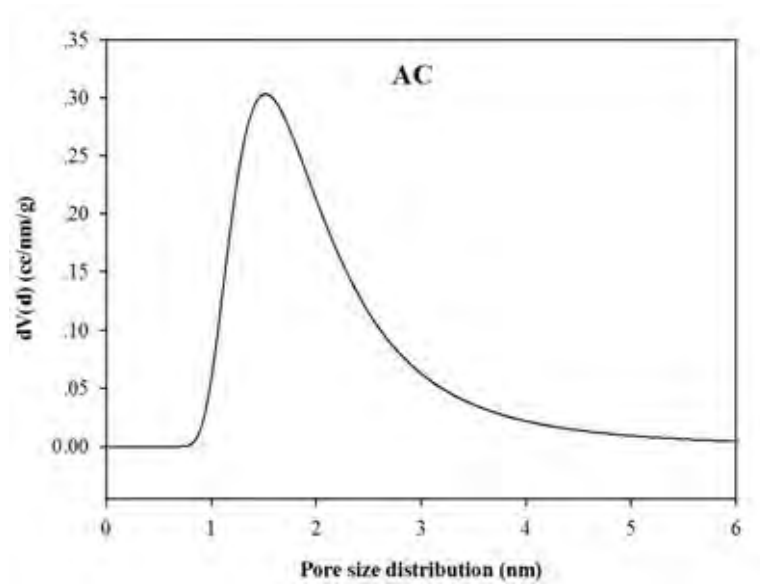## Appendix A Dubinin-Astakhov (DA) pore size distribution

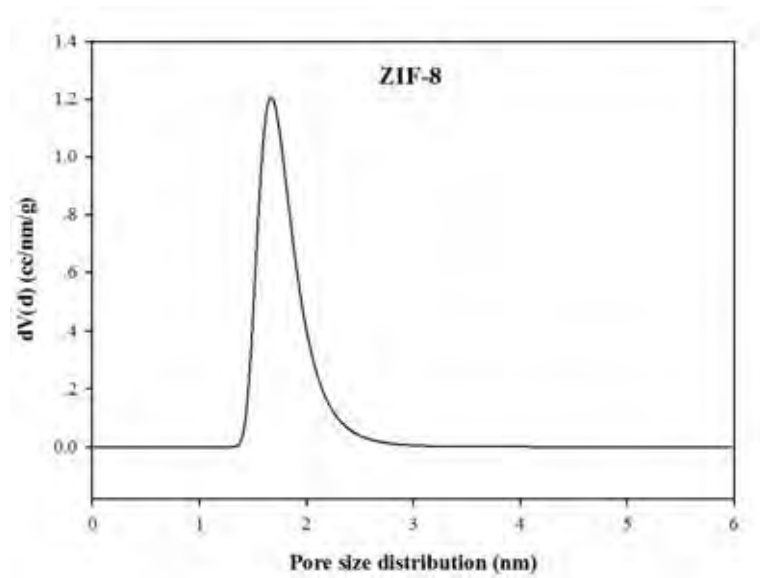**Figure A1** Micropore size distribution of activated carbon (AC).

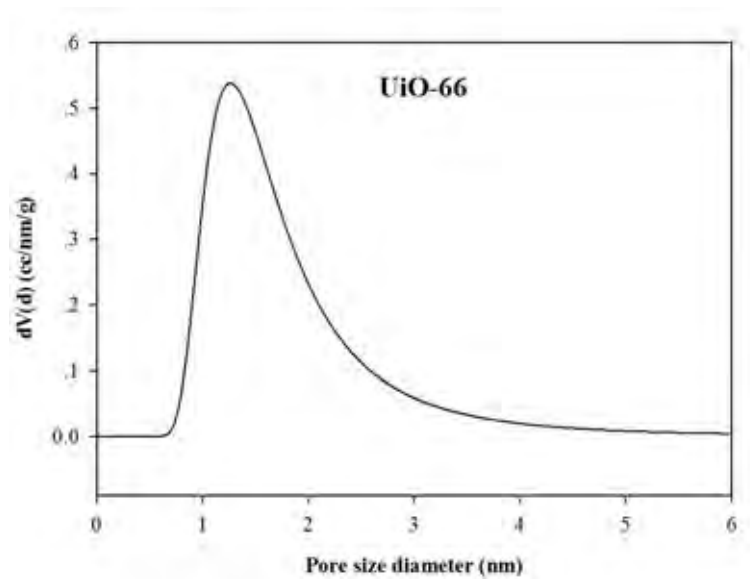**Figure A2** Micropore size distribution of ZIF-8.

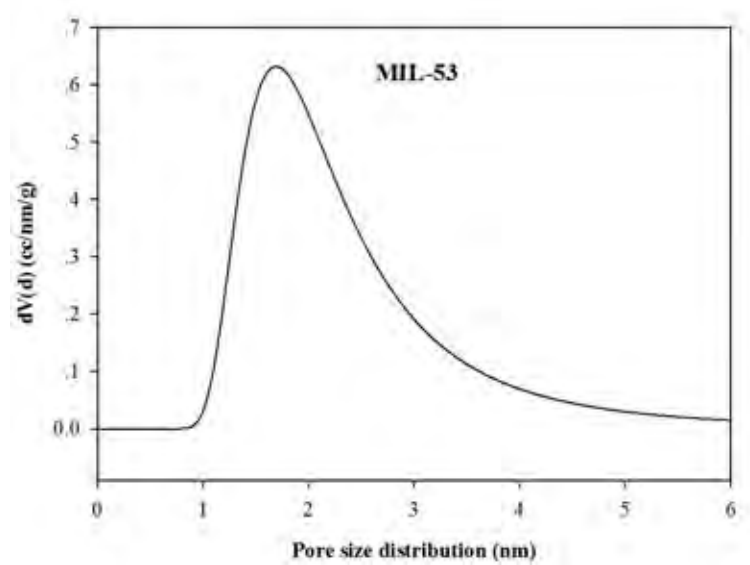**Figure A3** Micropore size distribution of UiO-66.

Figure A4 Micropore size distribution of MIL-53.

Appendix B Methane Adsorption on Different Adsorbents at 30 °C (± 2)

Table B1 The amount of methane adsorption capacity on activated carbon at 30 °C (± 2)

Equilibrium pressure (psia)	Methane adsorption (mmol/g)
13.13	0.00
23.82	0.04
33.44	0.17
43.57	0.25
53.69	0.32
63.69	0.41
74.38	0.49
84.01	0.58
93.63	0.66
103.26	0.71

Table B2 The amount of methane adsorption capacity on ZIF-8 at 30 °C (± 2)

Equilibrium pressure (psia)	Methane adsorption (mmol/g)
13.13	0.00
22.51	0.14
32.71	0.26
43.11	0.34
53.19	0.48
63.38	0.58
72.63	0.70
82.76	0.86
92.94	1.01
102.38	1.18

Table B3 The amount of methane adsorption capacity on UiO-66 at 30 °C (± 2)

Equilibrium pressure (psia)	Methane adsorption (mmol/g)
13.13	0.00
24.01	0.10
35.66	0.20
44.38	0.32
54.19	0.43
64.19	0.53
73.88	0.63
83.76	0.71
93.51	0.80
101.88	0.89

Table B4 The amount of methane adsorption capacity on MIL-53 (Al) at 30 °C (± 2)

Equilibrium pressure (psia)	Methane adsorption (mmol/g)
13.13	0.00
22.81	0.19
35.57	0.32
43.26	0.41
53.07	0.54
63.01	0.63
72.88	0.81
83.07	0.93
93.19	1.10
101.57	1.32

Table B5 The amount of methane adsorption capacity on 50 wt% activated carbon at 30 °C (± 2)

Equilibrium pressure (psia)	Methane adsorption (mmol/g)
13.13	0.00
27.07	0.00
37.24	0.03
46.41	0.05
54.81	0.08
64.27	0.10
73.96	0.12
84.67	0.16
95.19	0.21
103.94	0.25

Table B6 The amount of methane adsorption capacity on 25 wt% activated carbon at 30 °C (± 2)

Equilibrium pressure (psia)	Methane adsorption (mmol/g)
13.13	0.00
26.38	0.00
36.82	0.02
47.13	0.03
55.63	0.04
64.76	0.05
74.07	0.06
84.32	0.07
94.32	0.08
103.26	0.10

Table B7 The amount of methane adsorption capacity on 75 wt% ZIF-8 at 30 °C (± 2)

Equilibrium pressure (psia)	Methane adsorption (mmol/g)
13.13	0.00
23.59	0.05
33.59	0.13
44.07	0.17
53.88	0.25
63.90	0.32
73.34	0.45
83.17	0.61
93.01	0.72
103.15	0.85

Table B8 The amount of methane adsorption capacity on 50 wt% ZIF-8 at 30 °C (± 2)

Equilibrium pressure (psia)	Methane adsorption (mmol/g)
13.13	0.00
23.94	0.00
34.01	0.08
43.57	0.16
53.76	0.21
63.57	0.26
73.69	0.30
83.44	0.38
93.57	0.44
103.57	0.53

Table B9 The amount of methane adsorption capacity on 25 wt% ZIF-8 at 30 °C (± 2)

Equilibrium pressure (psia)	Methane adsorption (mmol/g)
13.13	0.00
22.51	0.00
33.51	0.05
43.76	0.08
53.69	0.12
63.88	0.18
73.76	0.22
83.88	0.27
93.32	0.30
103.51	0.33

Appendix C Carbon Dioxide Adsorption on Different Adsorbents at 30 °C (± 2)

Table C1 The amount of carbon dioxide adsorption capacity on activated carbon at 30 °C (± 2)

Equilibrium pressure (psi)	Carbon dioxide adsorption (mmol/g)
13.13	0.00
23.13	0.23
35.04	0.34
45.57	0.58
55.82	0.74
65.76	0.92
75.82	1.03
85.32	1.16
95.26	1.24
104.76	1.37

Table C2 The amount of carbon dioxide adsorption capacity on ZIF-8 at 30 °C (± 2)

Equilibrium pressure (psia)	Carbon dioxide adsorption (mmol/g)
13.13	0.00
22.76	0.55
34.76	0.71
44.76	0.89
54.82	1.10
64.57	1.37
74.44	1.65
84.32	1.83
94.38	1.98
104.13	2.12

Table C3 The amount of carbon dioxide adsorption capacity on UiO-66 at 30 °C (± 2)

Equilibrium pressure (psia)	Carbon dioxide adsorption (mmol/g)
13.13	0.00
21.13	0.92
33.63	1.24
42.69	1.56
52.26	1.81
62.88	2.04
72.69	2.27
82.72	2.45
93.32	2.63
103.57	2.80

Table C4 The amount of carbon dioxide adsorption capacity on MIL-53 (Al) at 30 °C (± 2)

Equilibrium pressure (psi)	Carbon dioxide adsorption (mmol/g)
13.13	0.00
20.70	0.80
33.04	1.21
42.35	1.59
52.34	1.97
62.54	2.30
72.32	2.60
82.21	2.86
93.04	3.06
103.57	3.25

CURRICULUM VITAE

Name: Ms. Chutima Sudsuansi

Date of Birth: September 18, 1993

Nationality: Thai

University Education:

2012–2016   Chulalongkorn University, Faculty of Science, Department of Chemical Technology, Bangkok, Thailand

Work Experience:

2015-2015   Position: Trainee

Company name: SCG Chemicals, Thailand

Presentations:

1. Sudsuansi, C., Kulpratipunja, S., Ratanatawanate, C., Rangsunvigit, P. (2018, August 25-29) Adsorption of Methane and Carbon Dioxide on Activated carbon and ZIF-8 (Zeolitic Imidazolate Framework). Proceeding of 21st Conference on Process Integration, Modelling and Optimisation, Prague, Czech Republic.

2. Sudsuansi, C., Kulpratipunja, S., Ratanatawanate, C., Rangsunvigit, P. (2018, May) Adsorption of Methane and Carbon Dioxide on Activated carbon and Metal Organic Frameworks. Proceeding of The 6th Research Symposium on Petroleum, Petrochemicals and Advanced Materials and The 21st PPC Symposium on Petroleum, Petrochemicals, and Polymers, Bangkok, Thailand.